© 1997 The Chemical Society of Japan

Bull. Chem. Soc. Jpn., **70**, 2861—2880 (1997)

Accounts

Dynamic Processes in Electrochemical Reactions Studied by Surface-Enhanced Infrared Absorption Spectroscopy (SEIRAS)

Masatoshi Osawa

Catalysis Research Center, Hokkaido University, Sapporo 060

(Received June 24, 1997)

Molecules adsorbed on evaporated thin metal films exhibit enormously strong infrared absorption. The thin metal films that exhibit the surface-enhanced infrared absorption (SEIRA) consist of metal particles much smaller than the wavelength of light. Electric field associated with the incident infrared radiation is enhanced via the excitation of localized plasmon of the particles, yielding the absorption enhancement. Preferential orientation and the change in absorption coefficient of molecules caused by chemisorption onto the metal surface provide additional enhancement. Most characteristic observations in SEIRA experiments are well explained by a simple electromagnetic theory. The infrared spectroscopy utilizing the SEIRA effect is promising as a new surface analytical tool. In particular, it is very useful for in situ studies of electrode/electrolyte interfaces. By the combined use of the attenuated-total-reflection technique, reactions and adsorption/desorption of molecules at the interfaces can be investigated at a high sensitivity without the interference from the bulk solution. The high sensitivity of this technique enables dynamic (or time-resolved) infrared monitoring of reactions and other time-dependent phenomena at the electrochemical interface at time-resolutions ranging from microseconds to milliseconds. Two-dimensional correlation analysis of time-resolved spectra highlights certain useful information that is not clearly seen in the usual one-dimensional spectra.

On certain rough metal surfaces, molecules show interesting spectroscopic phenomena that cannot be explained by classical theories. The most well-known phenomenon is surface-enhanced Raman scattering (SERS).[1—5] Molecules adsorbed on specially prepared metal surfaces show Raman scattering 10^4—10^6 times more intense than free molecules. Related phenomena such as surface-enhanced second-harmonic generation, four-wave mixing, absorption, and fluorescence have also been observed in the visible region.[1—5] Efforts to explain the surface-enhanced effects have led to an increased understanding of phenomena associated with the interaction of photon with adsorbates and metal surfaces. The surface-enhanced infrared absorption (SEIRA) described in this article is one of such phenomena observed in the infrared (IR) region.

In 1980, Hartstein et al.[6] reported for the first time that IR absorption of organic thin films on Si substrate is remarkably enhanced by evaporating Ag or Au thin films onto the organic films (metal-overlayer geometry). The enhancement was observed also by forming organic films on very thin metal films evaporated on Si (metal-underlayer geometry). However, it is not very clear whether they really observed the absorption enhancement because their measurements were limited only to the high frequency region above 2800 cm^{-1}. They observed three bands at 2850, 2925, and 2960 cm^{-1}, and assigned these bands to the CH stretching modes of aromatic molecules used as samples. However, aromatic molecules should exhibit CH stretching modes above 3000 cm^{-1} and the observed bands are undoubtedly assigned to the CH stretching modes of alkyl chains (probably, of hydrocarbon contaminants). Later on, Hatta et al.[7,8] traced the experiments and demonstrated very clearly, by the measurements of the finger print region, that the enhancement is not an artifact. Since the discovery, several research projects directed toward the understanding of the nature and mechanism of SEIRA were conducted in Japan in the 1980's,[9—17] which have been reviewed by Suëtaka.[18] Although considerable progress was made, these pioneering works did not receive intense interest.

Recently, SEIRA has become to receive a renewed interest due to the development of its applications. This movement was triggered by experimental and theoretical studies of the enhancing mechanisms by Osawa et al,[19—21] and by series of works by Nishikawa et al.[22—27] on the application to trace analysis of chemical compounds. The first symposium on SEIRA was held at the 1997 Pittsburgh Conference (March, Atlanta).

The IR spectroscopy using the SEIRA effect (SEIRAS) is very promising as a tool to characterize adsorbed molecules on metal surfaces. The so-called IR reflection-absorption spectroscopy (IRAS) is the most well-known technique for acquiring IR spectra of molecules adsorbed on metal surfaces.[18,28] SEIRAS has a sensitivity by a factor of 10—50 higher than IRAS.[21,29] Since IRAS has a sensitivity high enough to detect monolayer adsorbates, one might think that the difference in sensitivity is not very important. However, it must be noted that the signal-to-noise ratio of a spectrum is proportional to the square root of the coadded number of interferograms in Fourier transform (FT) IR spectrometry. In IRAS measurements of monolayer adsorbates, hundreds to thousands of interferograms are required to be averaged to enhance the signal-to-noise ratio of a spectrum. In SEIRAS measurements, on the other hand, the same signal-to-noise ration as IRAS is expected to be obtained without interferogram averaging or with averaging of a smaller number of interferograms, on the basis of the simple calculation. In this point of view, SEIRAS is suitable for time-resolved monitoring of reaction processes at surfaces and interfaces. Fortunately, recent developments of step-scan and rapid-scan FT-IR instrumentation have enabled to study time-dependent phenomena at time-resolutions ranging from nanoseconds to milliseconds.[30] By the combined use of SEIRAS and the time-resolved FT-IR interferometry, significant progress has been made in time-resolved in situ monitoring of electrochemical reactions.[31,32]

Recent research in electrochemistry has increasingly involved the use of surface-sensitive analytical techniques in combination with electrochemical techniques.[33—35] The chief reason for this development is that electrochemical techniques inevitably measured the sum of all surface processes. The results provide kinetic information primarily, such as the rate of reaction and the influences of diffusion, concentration, temperature, etc., on the rate. No structural information is obtained regarding the interface and surface species involved in reactions. On the other hand, newly developed in situ techniques, including scanning tunneling microscopy (STM), surface X-ray spectroscopy, IRAS, and SERS, provide detailed information on the structures of electrode surfaces and adsorbed molecules. The atomic and molecular scale approach are reforming our image of the electrochemical interface.[33—35]

Nevertheless, it is very important to point out that such microscopic level measurements have been carried out separately from electrochemical measurements in the most cases. Namely, the former measurements are carried out under static conditions (at static potentials), whereas electrochemical measurements are usually carried out under potential sweep or modulated conditions. For direct comparison of the structural information obtained by the modern techniques and the kinetic information obtained by conventional electrochemical techniques, both measurements must be carried out simultaneously at suitable time-resolutions. The time-resolution required for electrochemistry is from nanoseconds to milliseconds in most cases, since the response of the interface for externally applied potential perturbations is limited to this time-region by the responses of electrochemical equipments or by the charging of the electric double-layer at the interface. The present time-resolved FT-IR interferometry cover this time-region.

This article is devoted to review recent developments in the SEIRAS made in our own laboratory. The nature and the mechanism of SEIRA is described in Part 1 and Part 2, respectively. In Part 3, the application of SEIRAS to electrochemistry is described. Studies on the adsorption of molecules onto electrode surface, electrochemical reactions, and the potential-dependent reorientation of water molecules at the electrochemical interface are mentioned, through which the utilities of SEIRAS are demonstrated. Time-resolved measurements of reactions and dynamics are highlighted. The application of two-dimensional IR technique, that is very useful to extract certain information from time-resolved spectra, is also described.

1. The Nature of SEIRA

An example of SEIRA experiments is shown for *p*-nitrobenzoic acid (PNBA) adsorbed on Ag. Figure 1a shows transmission spectra of thin PNBA films formed on Ag films of various thicknesses (d_{Ag}) ranging from 0 to 14 nm. The metal films were prepared by vacuum evaporation onto CaF_2 disks. The thickness of the metal film is mass thickness

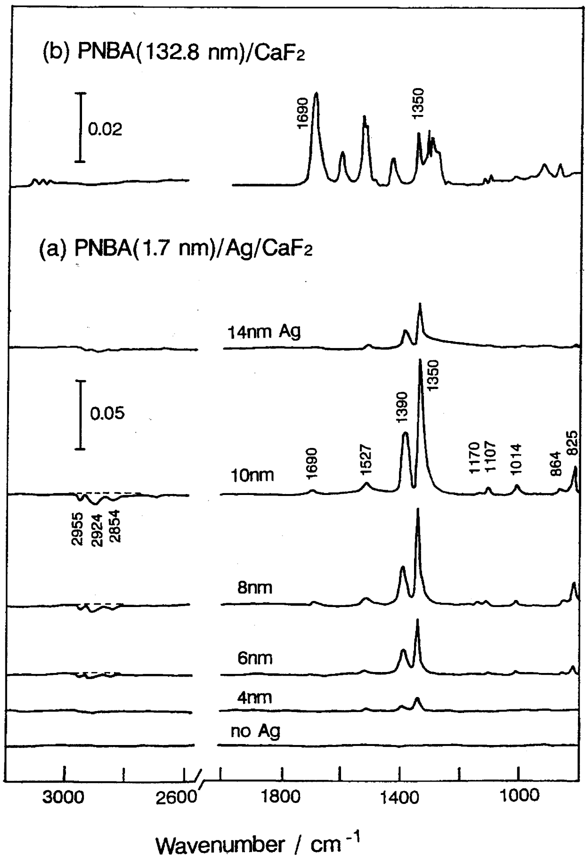

Fig. 1. Transmission infrared spectra of *p*-nitrobenzoic acid (PNBA) films deposited on (a) Ag-coated and (b) bare CaF_2 substrates. Mass thicknesses of the Ag films are shown in the figure. The thickness of the organic films is 1.7 nm (a) or 132.8 nm (b).

(d_{mass}) measured with a quartz crystal microbalance. The organic films were formed by dropping an acetone solution onto the metal surfaces and then by vaporizing the solvent. The thickness of the PNBA film (d_{PNBA}), evaluated from the concentration and the volume of the solution dropped on the surface, is 1.7 nm for all the samples. The background absorption of the metal films, acquired before the deposition of the organic films, was subtracted from each spectrum. For comparison, the spectrum of a thick PNBA film of d_{PNBA} = 132.8 nm formed on a bare CaF_2 substrate (without a metal film) is shown in Fig. 1b. Relative band intensities in the spectrum were the same as those in the spectrum of the powder sample (not shown), implying that the molecules are randomly oriented in the thick film deposited on the bare substrate.

It is clearly seen from Fig. 1a that the absorption of the molecule is remarkably enhanced in the presence of the Ag underlayers. No bands are detectable for the very thin organic film directly deposited onto the bare substrate ($d_{Ag} = 0$ nm). As the thickness of Ag increase, two strong bands appear at 1390 and 1350 cm^{-1}, and grows in intensity. The 1390 cm^{-1} band is missing in the reference spectrum (Fig. 1b) and is assigned to the symmetric COO^- stretching (ν) mode, ν_sCOO^-, of carboxylato group of the molecule ($PNBA^-$), suggesting that the molecule is chemisorbed onto Ag via the carboxyl group by dissociating its proton. The 1350 cm^{-1} band is assigned to the symmetric NO_2 stretching mode, ν_sNO_2, which is common for both PNBA and $PNBA^-$. The weak band at 1690 cm^{-1} is assigned to the νC=O mode of the undissociated molecule (acid). The three negative-going bands around 2900 cm^{-1} are assigned to νCH modes of hydrocarbon contaminants as described above. The contaminants are removed from the surface by the chemisorption of PNBA, yielding negative sign. If we assume that the absorption coefficient of the ν_sNO_2 mode does not change upon chemisorption, the enhancement factor is calculated to be about 30 at $d_{Ag} = 4$ nm and 500 at $d_{Ag} = 10$ nm from the comparison of the peak intensities in the enhanced and reference spectra, by taking into account the difference in thickness of the organic films.

The infrared absorption enhancement has been observed for a variety of molecules and ions adsorbed onto vacuum evaporated thin metal films such as Ag, Au, Cu, In, Pt, Pd, Ni, Al, and Pb. In general, Ag and Au exhibit the most intense enhancement. The nature of SEIRA observed so far is summarized below.

(1) Island Structure of Thin Metal Films. It is well known that very thin noble metal films evaporated on nonmetallic substrates are not continuous, but consist of small islands (particles). The average dimensions of islands observed by a scanning electron microscope (SEM) were about 30 nm in diameter and 10 nm in height for a 10 nm-thick Ag film evaporated on Si. The islands grow with increasing average thickness and eventually form a uniform film.

The enhancement factor changes greatly depending upon the island structure of the metal film. Figure 1a shows that the enhancement is a strong function of the thickness of the metal film. With increasing d_{Ag}, band intensities increase, reach maxima around 10 nm, and then sharply decrease. SEM observations of the metal films revealed that metal islands are well separated with each other at $d_{mass} \leq 10$ nm and are contacting each other at $d_{Ag} = 14$ nm, suggesting that the island structure plays an important role in SEIRA. The total surface area of the islands, estimated from SEM observations, was larger than the geometrical area of the substrate by a factor of about three for $d_{Ag} = 6$ and 14 nm, and by a factor of about five for $d_{Ag} = 10$ nm. The difference in the surface area is much too small to explain the observed strong d_{Ag}-dependence of the enhancement.

The d_{Ag}-dependence of the enhancement is greatly affected by the deposition rate of the metal.[36)] In Fig. 2, the intensities of the ν_sNO_2 band of PNBA on Ag films deposited at different rates are shown as a function of d_{Ag}. The optimal thickness increases from 10 to 20 nm as the deposition rate decreases from 0.1 to 0.001 nm s^{-1}. Slower deposition gives larger enhancement. Temperature and surface properties of the substrate also affect the enhancement.[36)] As the substrate temperature increases, the enhancement decreases. All these findings were ascribed to differences in shapes and size of islands.

(2) Surface Selection Rule. In the spectrum of potassium salt of PNBA (KBr pellet), the antisymmetric COO^- and NO_2 stretching modes are observed at 1590 and 1540 cm^{-1}, respectively, as strong as the corresponding symmetric modes.[21)] Nevertheless, these antisymmetric modes are completely missing in the enhanced spectra shown in Fig. 1a. The same spectral patterns are observed in the IRA spectrum of the molecule chemisorbed onto a bulk Ag surface (smooth surface).[21)] In IRAS, the standing electric field at the surface formed via the interaction between the incident and reflected beams is polarized along the surface normal, and therefore only the molecular vibrations that have dipole changes normal to the surface give absorption.[18,28)] On the basis of the surface selection rule, it is concluded that the molecule is oriented with its molecular axis (C_2 axis) normal to the sur-

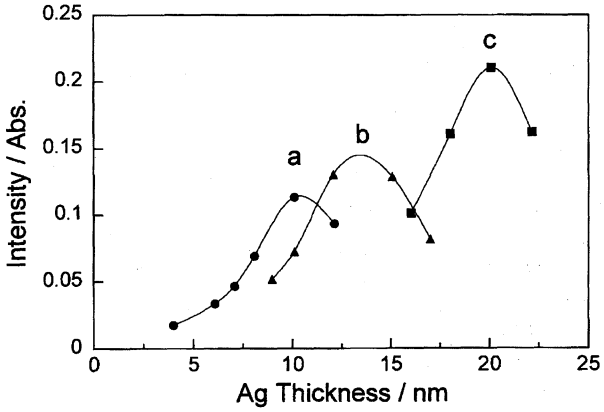

Fig. 2. Peak intensity of the 1350 cm^{-1} band of PNBA adsorbed on evaporated Ag films as a function of the metal thickness. The deposition rates of the Ag films are (a) 0.1, (b) 0.05, and (c) 0.001 nm s^{-1}. The substrate is BaF_2. The curves are drawn by eye guide.

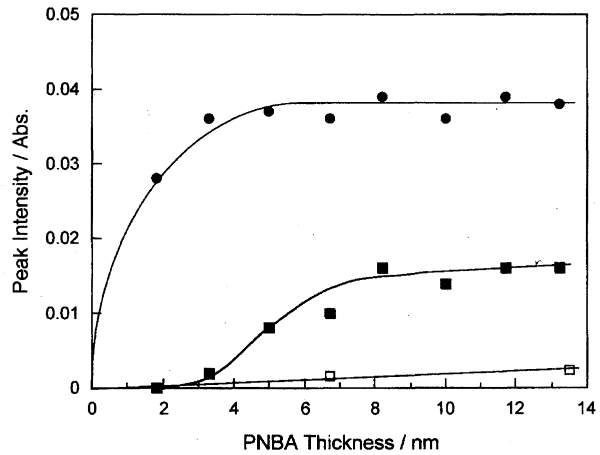

Fig. 3. Peak intensity of the 1390 and 1690 cm^{-1} bands (closed circles and squares, respectively) of PNBA adsorbed on a 10 nm-thick Ag film evaporated on $\mathrm{CaF_2}$ as a function of the thickness of the organic layer. Open square is the intensity of the 1690 cm^{-1} band for the organic layer deposited on the bare substrate. The curves are drawn by eye guide.

face. The spectra shown in Fig. 1a imply that SEIRAS has the same surface selection rule as IRAS. However, the presence of the surface selection rule in SEIRAS seems to be very strange because metal films have island structures and molecular orientation on island films is random at a macroscopic scale even if molecules are preferentially oriented with respect to the local surfaces of the metal islands. This puzzle is explained if we assume that the electric field that excites the adsorbate vibrations is normal to the local surfaces of metal islands at any point.

(3) Spatial Range of the Enhancement. In conventional transmission measurements, band intensity linearly increases as the thickness of a sample film increases (Lambert–Beer's law). In SEIRA experiments, on the other hand, intensity is not a linear function of film thickness. In Fig. 3, the intensities of the $\nu_s\mathrm{COO^-}$ (closed circles) and $\nu\mathrm{C{=}O}$ bands (closed squares) of chemisorbed and physisorbed PNBA, respectively, on a 10 nm-thick Ag film are plotted as a function of d_{PNBA}.[19] The intensity of the $\nu_s\mathrm{COO^-}$ band rises sharply with increasing d_{PNBA} and saturates at about 3 nm, suggesting that full monolayer coverage is reached. After the saturation of the $\nu_s\mathrm{COO^-}$ band, the $\nu\mathrm{C{=}O}$ band appears and increases in intensity with increasing film thickness. The gradient of the intensity vs. d_{PNBA} curve for the $\nu\mathrm{C{=}O}$ band is relatively large at $d_{\mathrm{PNBA}} = 3$—8 and eventually approaches to that for the same band of PNBA films deposited on a bare substrate (open squares). The enhancement factor, estimated from the ratio of the gradients with and without the metal film, is 20—30 at $d_{\mathrm{PNBA}} = 3$—8 nm. The data indicate that the enhancement is significant for the chemisorbed first layer and decays as the distance from the surface increases. The distance-dependence was investigated in more detail by using Langmuir–Blodgett (LB) monolayers as spacers, and it was shown that the enhancement diminishes within about 5 nm from the surface.[13,37,38]

(4) Incident Angle-Dependence of the Enhancement in External and Internal Reflection Measurements. The enhanced absorption is observed in external reflection and attenuated-total-reflection (ATR) geometry as well. In these experiments, band intensities greatly change upon incident angle and polarization of the incident IR radiation. Figure 4 shows a series of SEIRA spectra of PNBA adsorbed on a 5 nm-thick Ag film acquired with the external-reflection geometry. The substrate is $\mathrm{BaF_2}$ (reflective index $n = 1.42$). For *s*-polarization, vibrations of the adsorbed molecule are observed as negative-going bands (increase of reflectivity) regardless of incident angle. For *p*-polarization, on the other hand, absorption is negative at incident angles below 45° and positive above 55°. The change in sign occurs near the Brewster angle ($\theta_B = \tan^{-1}(n) = 54.8°$).[39] The enhancement is the largest around θ_B for *p*-polarization, but the signal-to-noise ratio of the spectrum is worse than at other angles, since the reflectivity of the substrate is very low around θ_B. The same results have been obtained on other nonmetallic substrates such as glass, semiconductors, and polymers.[39] Enhancement is observed also by evaporating a thin metal film onto a sample film. A very excellent SEIRA spectrum of a LB monolayer transferred onto a slide glass has been obtained with the metal-overlayer external reflection configuration.[39] However, no enhancement is observed when a LB film is formed on a metal mirror and then a thin metal film is evaporated on it.[13]

The incident angle-dependence of the enhancement in ATR geometry is shown in Fig. 5, where the intensity of the $\nu_s\mathrm{NO_2}$ band of PNBA adsorbed on Ag films is plotted as a function of incident angle θ. A Ge hemicylindrical prism ($n = 4.0$) was used as the ATR element. For a 5.5 nm-thick Ag film (a), the intensity is maximal at the critical angle of total reflection ($\theta_c = \sin^{-1}(1/n) = 14.18°$) for *s*-polarization (open circles) and decreases gradually as the incident angle increases. Almost the same angle-dependence is observed for *p*-polarization (closed circles), but note that the intensity decreases as the angle approaches close to θ_c. For a 12 nm-thick Ag film (b), on the other hand, the enhancement is observed only for *p*-polarization and is maximal at a high incident angle around 80°.

(5) Background Absorption by Metal Films. The enhanced IR bands are superposed on a very broad and strong background absorption by metal island films ranging from the visible to IR regions.[19] Figure 6 shows a series of transmission spectra of Ag films of various thicknesses evaporated on $\mathrm{CaF_2}$, which are acquired by using the spectrum of bare substrate as the reference. When d_{Ag} is very small, a sharp band is observed around 500 nm. This band becomes broader and shifts to the near-IR region as d_{Ag} increases. The tail of the absorption band is extending well into the mid-IR region. The dashed curve in the figure represents the transmittance of a hypothetical continuous Ag film (10-nm in thickness) calculated with the Fresnel formula[40] and the dielectric function of bulk Ag. The observed background spectra are markedly different from the calculation. The enhanced absorption of the adsorbed molecule is proportional

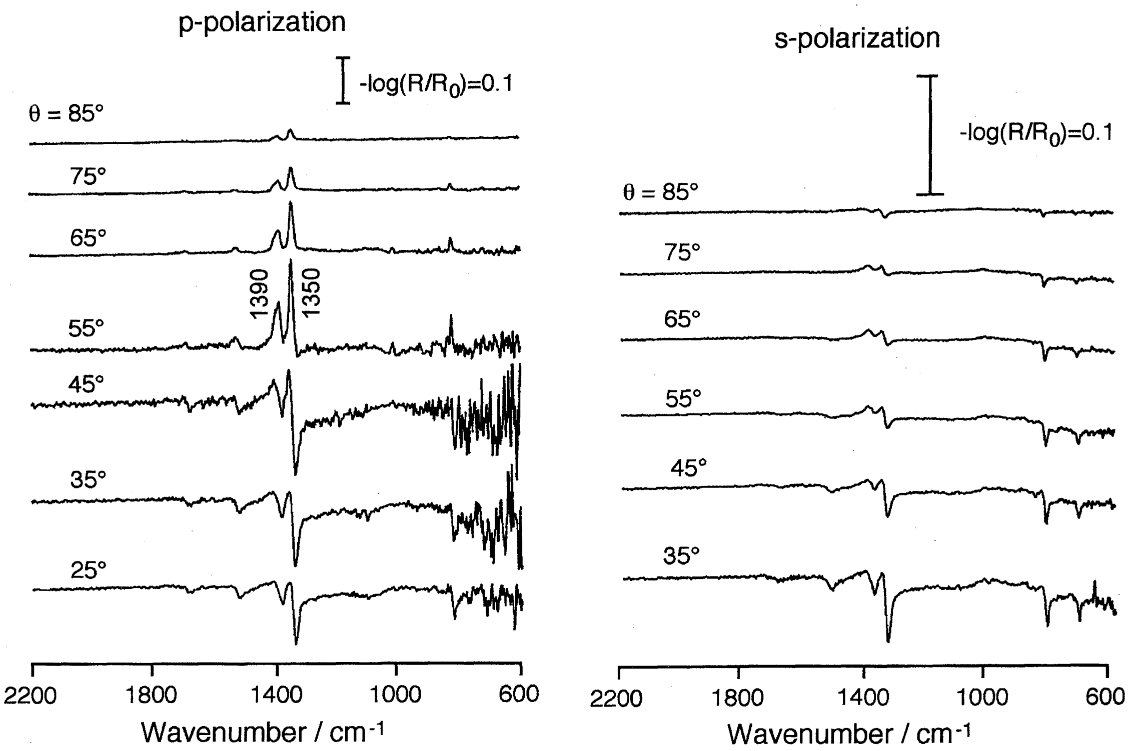

Fig. 4. External reflection SEIRA spectra of a 4 nm-thick PNBA film deposited on a Ag coated BaF_2 for *p*- and *s*-polarization. Mass thickness of the Ag film is 5-nm. Incident angle (θ) of the infrared radiation is shown in the figure.

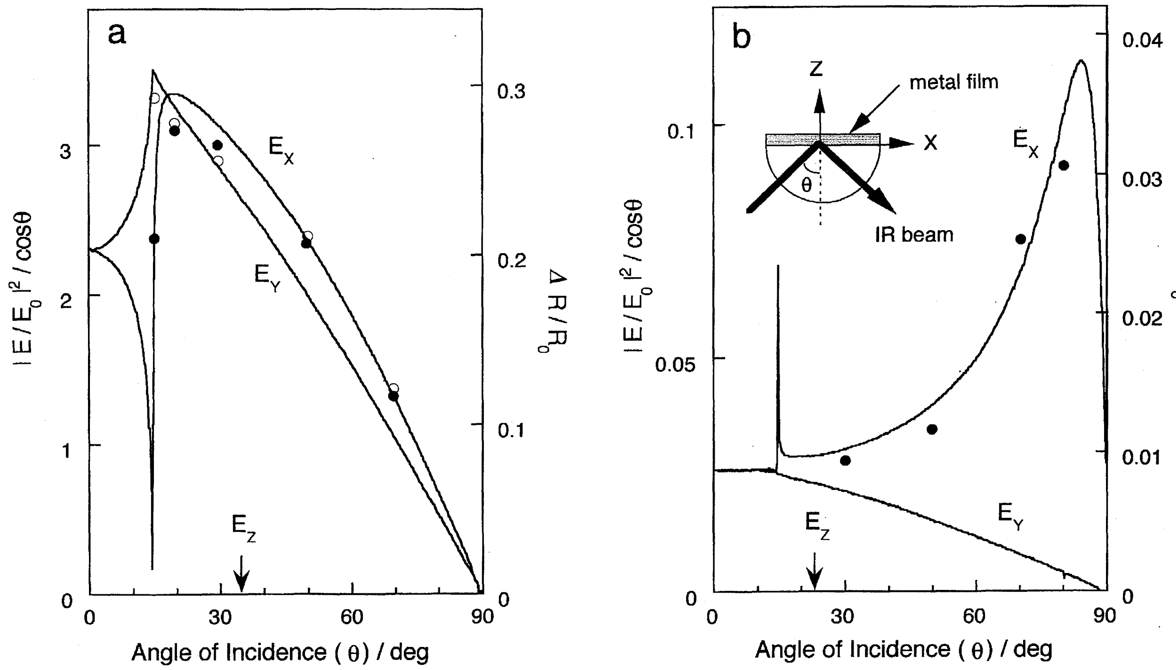

Fig. 5. Peak intensity of the 1350 $\mathrm{cm^{-1}}$ band of PNBA adsorbed on Ag island films of $d_{\mathrm{mass}} = 5.5$ and 12 nm (a and b, respectively) measured with the ATR configuration as a function of incident angle (θ) for *p*- and *s*-polarization (closed and open circles, respectively). The solid lines represent the *X*-, *Y*-, or *Z*-components of the mean square electric field intensity within the metal films. See text on the details.

to the background absorption in the mid-IR region.[19]

2. Mechanisms of SEIRA

Island films of coinage metals that exhibit intense SEIRA are good enhancers also for Raman scattering. The nature of SEIRA mentioned above is very similar to that of SERS observed on island films,[41] suggesting that the enhancing mechanisms of SEIRA are similar to those of SERS. The

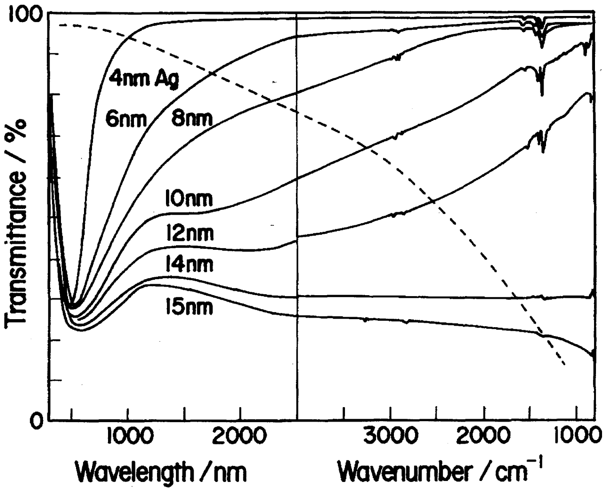

Fig. 6. Transmission spectra of Ag island films evaporated on CaF_2. The spectrum of a bare substrate was used as the reference. Mass thickness of Ag is shown in the figure. The metal films are coated with 1.7 nm-thick PNBA films. The dashed trace is the transmission spectrum of a hypothetical parallel-sided continuous Ag film (10 nm in thickness) calculated with the Fresnel formula and the dielectric function of bulk Ag.

mechanisms of SERS have been investigated extensively; they are well-documented in several review articles.[1—5] It is well-established that the overlap of "electromagnetic" and "chemical" mechanisms yields enhancement factors of 10^4—10^8 for SERS. The electromagnetic mechanism is that the electric field associated with the incident laser radiation is enhanced through the coupling with various plasmon modes of the metal. The enhanced electric field can strongly excite the adsorbed molecules, yielding the enhanced Raman scattering. Raman scattered radiation is also enhanced by the coupling with such modes, which provides further net enhancement. In other word, the metal surface functions as an antenna which enhances both excitation light and Raman scattered light. On the other hand, the chemical mechanism is ascribed to the increase in polarizability of molecules caused by chemisorption onto the metal surface. A kind of resonance Raman scattering occurs associated with the photoinduced charge transfer between the adsorbed molecules and the metal.[1—5,42,43]

2.1. Electromagnetic Mechanism for SEIRA. The incident angle-dependence of the enhancement in the ATR measurements (Fig. 5) is well-correlated with the intensity of the electric field produced by the interference of light.[9,15] The solid lines in Fig. 5 are the mean square electric field intensity (MSEFI) within the metal film, $|E|^2$, calculated by means of the Fresnel equations under an assumption that the metal film is a plane-parallel continuous film. To take into account the island nature of the film, the dielectric function of the hypothetical film, ε_{BR}, was calculated by the Bruggeman effective medium approximation[44]

$$F\frac{\varepsilon_m-\varepsilon_{BR}}{\varepsilon_m+2\varepsilon_{BR}}+(1-F)\frac{\varepsilon_h-\varepsilon_{BR}}{\varepsilon_h+2\varepsilon_{BR}}=0, \qquad (1)$$

where ε_h is the dielectric constant of the host medium surrounding the metal islands (= air), ε_m the dielectric function of the bulk metal, and F the volume fraction of the metal in the hypothetical film defined as the ratio of mass and optical thicknesses of the film (d_{mass}/d_{opt}). The subscript X, Y, or Z of E denotes the component along the X, Y, or Z axis, respectively (see the coordination system in Fig. 5). p-Polarized radiation gives X- and Z-components, whereas s-polarization gives Y-component only. For the comparison with the experimental data, MSEFI was normalized to the incident light, $|E_0|^2$, and was also divided by cos θ in order to take into account the increase in the irradiated area (namely, the number of molecules to be sampled) with increasing incident angle θ.

The calculation shows that the Z-component is negligible and the field is essentially in the plane of the film, the X–Y plane, regardless of the polarization of the light. The observed angle-dependencies of the enhanced IR absorption for p- and s-polarization are the same as those of the X- and Y-components of the MSEFI, respectively. The intimate relation between the enhancement and electric field intensity strongly argues that a certain electromagnetic mechanism is contributing to the IR enhancement. The MSEFI is similar to or smaller than the incident electric field intensity, and does not explain the enhancement. However, it is noted that the value calculated here is the average field intensity within the effective medium. Remembering that the enhancement decays within a few monolayer distances from the surface (Fig. 3), there exists a possibility that the electric field is enhanced only in the very near vicinity of the islands. In the visible region, a short-ranged strong electric field is produced around metal islands via the excitation of localized plasmon (or collective electron resonance) of metal islands, which dominantly contributes to the SERS on evaporated metal films.[1—4,41] By the analogy with SERS, the enhanced local field around the islands is expected to play a role also in SEIRA.

The strong absorption in the visible and near-IR regions in the spectra shown in Fig. 6 is assigned to the excitation of localized plasmon modes.[1—4,45] The broadening and red shift of the peak associated with increase in d_{Ag} has been explained by dipole interactions between islands.[45,46] Laor and Schatz[46] calculated the enhancement of the electric field on rough Ag surfaces by modeling the rough surface as a set of metal particles. Chew and Kerker[47] calculated the enhancement of electric field in small cavities within metal films (mirror image of particles). These calculations showed that the electric field is enhanced on rough metal surfaces and in cavities by a factor of 10^2—10^6 in both the visible and near-IR regions. The validity of these calculations has been confirmed by the observation of SERS in the near-IR region (with the 1.064 μm excitation from a Nd : YAG laser) as strong as in the visible region.[48,49] Although the calculations are limited to the visible and near-IR regions, the electric field enhancement is expected also in the mid-IR region, since the absorption of the metal islands is extending well into the mid-IR region (Fig. 6).

The localized plasmon model is very suitable to explain several aspects of SEIRA.[20,21] Metal islands are polarized in the incident radiation via the localized plasmon excitation. Since the island dimension d is much smaller than the wavelength λ, i.e., in the Rayleight limit $2\pi d \ll \lambda$, the dipole moment p induced at the center of an island can be written as[3,50]

$$p = \alpha V E, \tag{2}$$

where α and V are the polarizability and the volume of the metal island, respectively, and E is the amplitude of the incident electric field. This dipole produces an electric field around the island[1—4,50] and excites adsorbed molecules. The intensity of the local electric field is written as[3,50]

$$|E_{\mathrm{local}}|^2 = 4p^2/l^6, \tag{3}$$

where l is the distance from the center of the island. This equation indicates that the local electric field decays within a short distance from the surface, which explains the observed short-ranged enhancement (Fig. 3).

On the bases of SEM observations, an island film can be modeled as a set of rotating ellipsoids as illustrated in Fig. 7. The rotating axis is normal to the substrate surface. Note that the local electric field is normal to local surfaces of the island.[50] Thereby, only the molecular vibrations that give dipole changes normal to local surfaces can be excited, yielding the surface selection rule. Localized plasmon is excited only along the major axis of the ellipsoids in the visible and near IR regions[45] (and probably also in the mid-IR region). Since the major axis is parallel to the substrate surface, the enhancement is observed in the transmission geometry (the electric field is normal to the direction of propagation). In the ATR geometry, the electric field parallel to the substrate surface (the X- and Y-components of MSEFI) can give the absorption enhancement (Fig. 5). It is also the case in the external reflection geometry.[39] When the substrate is highly reflective, however, no enhancement is observed in the external reflection geometry[13] because the electric field that excites metal islands is polarized normal to the substrate surface[18,28] (namely, along the semi-major axes of islands).

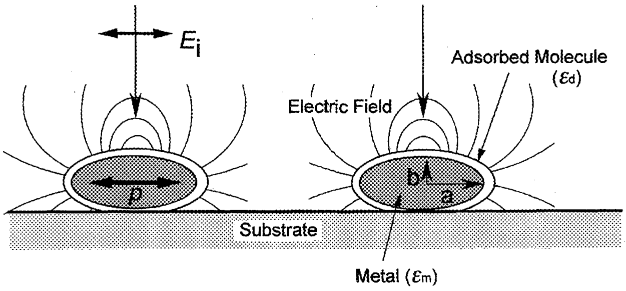

Fig. 7. Polarization of metal islands by the incident IR radiation and the electric field around the islands produced by the polarization. The islands are modeled by rotating ellipsoids with dielectric function of ε_{m}. The adsorbed molecule is modeled by a thin layer with dielectric function of ε_{d} covering the ellipsoids. The aspect ratio of the ellipsoid is defined as $\eta = a/b$.

The vibrations of adsorbed molecules excited by the enhanced local field also polarize the metal island, resulting in the perturbation of polarizability of the island at frequencies of the molecular vibrations. The image dipole induced in the island by oscillating dipoles of adsorbed molecules may also contribute to the perturbation.[51] The polarizability α of an island coated by a dielectric layer (adsorbed layer) is given by[20,21,52]

$$\alpha_{\|,\perp} = \left\{ \frac{(\varepsilon_{\mathrm{d}}-\varepsilon_{\mathrm{h}})[\varepsilon_{\mathrm{m}}L_1+\varepsilon_{\mathrm{d}}(1-L_1)]+Q(\varepsilon_{\mathrm{m}}-\varepsilon_{\mathrm{d}})[\varepsilon_{\mathrm{d}}(1-L_2)+\varepsilon_{\mathrm{h}}L_2]}{[\varepsilon_{\mathrm{d}}L_2+\varepsilon_{\mathrm{h}}(1-L_2)][\varepsilon_{\mathrm{m}}L_1+\varepsilon_{\mathrm{d}}(1-L_1)]+Q(\varepsilon_{\mathrm{m}}-\varepsilon_{\mathrm{d}})(\varepsilon_{\mathrm{d}}-\varepsilon_{\mathrm{h}})L_2(1-L_2)} \right\}_{\|,\perp}, \tag{4}$$

where ε_{m}, ε_{d}, and ε_{h} are the dielectric functions of the metal, adsorbed molecule, and host medium, respectively. Q is the volume ratio of the core (1) and coated (2) particles ($=V_1/V_2$), through which the size of the island and the thickness of the adsorbed layer are incorporated into the calculation. L_1 and L_2 represent depolarization of the core and coated ellipsoids, respectively, and are tabulated in Ref. 53 as a function of the aspect ratio of the ellipsoid, η ($= a/b$; a and b are radii along the major and semimajor axes of the ellipsoid, respectively. See Fig. 7). The subscript $\|,\perp$ of α refer to the applied field being parallel ($\|$) or perpendicular ($\perp$) to the substrate (the depolarization factor is different for different directions of the electric fields).

Since island dimensions are much smaller than the wavelength of IR radiation, it may be reasonable to assume an island film to be a parallel-sided continuous composite layer consisting of metal particles, adsorbed molecules, and host medium. If the spatially averaged (or effective) dielectric function of the composite layer can be estimated, transmittance and reflectance of the composite layer in trasmission, ATR, and external reflection modes can be calculated by the Fresnel equations.[20,21,29,39]

In the Maxwell–Garnett (MG) effective medium approximation theory,[44] the effective dielectric function of the composite layer, $\varepsilon_{\mathrm{MG}}$, is related to the polarizability of a particle by

$$\varepsilon_{\mathrm{MG}} = \varepsilon_{\mathrm{h}} \left(\frac{3+2F\alpha}{3-F\alpha} \right), \tag{5}$$

where F is the filling factor defined by $d_{\mathrm{mass}}/d_{\mathrm{opt}}$.

The MG model includes interactions between the particles only through the Lorentz field and provides a good description of physical properties of evaporated island films when mass thickness is small and islands are well separated. When islands are densely crowded, dipole interactions between islands become significant (see Fig. 6) and the Bruggeman (BR) model gives a better approximation. In the BR model, the effective dielectric function, $\varepsilon_{\mathrm{BR}}$, is given by[44]

$$\varepsilon_{\mathrm{BR}} = \varepsilon_{\mathrm{h}} \frac{3(1-F)+F\alpha'}{3(1-F)-2F\alpha'}. \tag{6}$$

The metal particles are assumed to be embedded in an effective medium in this mode and the polarizability α' is given by replacing ε_{h} in Eq. 4 by $\varepsilon_{\mathrm{BR}}$. It is noted that Eq. 1 is obtained from Eqs. 4 and 6 by taking $Q=1$ and $L_1=L_2=1/3$ (sphere).

In the simulations of enhanced IR spectra shown below, the dielectric constant of the host medium ε_h was taken to be 1 (air). The Drude model[50,54] was used to calculate the dielectric function of the metal. The dielectric function of the adsorbed molecule was simulated by the damped harmonic oscillator approximation.[55]

Figure 8a shows the calculated transmission spectra of a model molecule adsorbed on a Ag island film of d_{mass} = 5 nm (F = 0.5) on CaF_2 substrate (n =1.4).[21] The effective dielectric function was calculated with the MG model (Eq. 5). The thickness of the molecular layer and the size of the metal particles ($2a$) were assumed to be 1 nm (approximately one monolayer thickness) and 25 nm, respectively. The background without a molecular layer was subtracted from each spectra. For comparison, the simulation for the molecular layer on bare CaF_2 (without a metal film) is shown in the figure by a dashed trace. The calculation demonstrates that the enhancement depends on the shape of the island (namely, η). The intensity is as small as that without an island metal film for η =1 (sphere), and increases as η increases. The enhancement factor is 13 for η =3 determined by SEM. The calculated enhancement factor is smaller than the experimentally observed value (ca. 70) for chemisorbed PNBA on a Ag film of d_{mass} = 5 nm. However, one should note that the chemisorbed molecules are oriented with its molecular axis normal to the surface, whereas the molecules are randomly oriented in the film deposited on the bare substrate that is used as the reference in the estimate of the enhancement factor. The preferential orientation should give an additional enhancement for vibrational modes that have dipole changes along the surface normal (e.g., the symmetric modes for PNBA on Ag) by a factor of three compared with random orientation. By taking the orientation effect into account, an enhancement factor of about 40 ($=13\times3$) is expected.

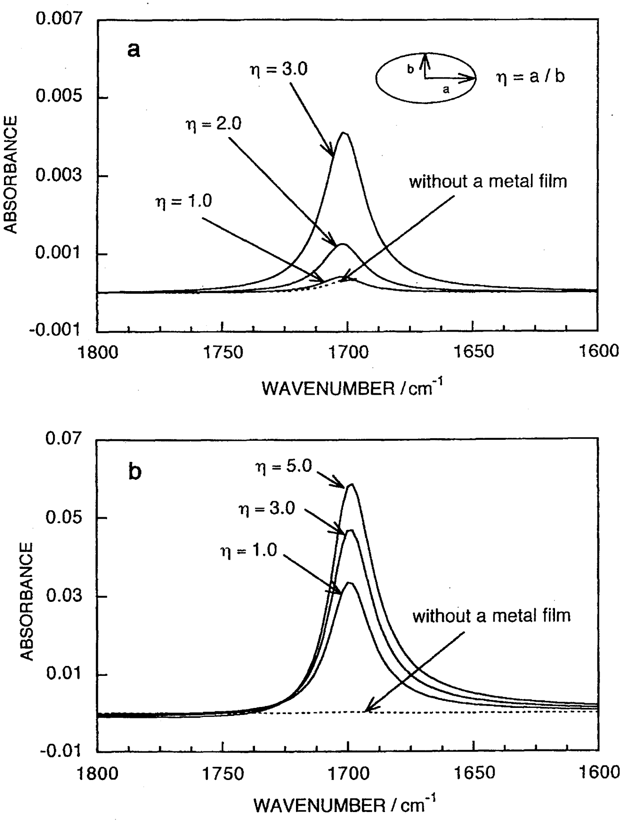

Fig. 8. Simulated transmission SEIRA spectra of a model molecular layer (d_{mol}=1 nm) on a Ag island films of d_{mass}=5 and 8 nm (a and b, respectively). The effective dielectric function of the metal-molecule-air composite film was calculated with Maxwell–Garnett (a) or Bruggeman (b) effective medium approximation. The dashed trace is the spectrum without an island metal film. The substrate is CaF_2. η represents the aspect ratio of the metal ellipsoid. See the text on the details of the calculation.

Figure 8b shows the transmission spectra of the same model molecule on a Ag island film of d_{mass}=8 nm (F = 0.7) calculated with the BR model.[21] The BR model gives a larger intensity than the MG model. The enhancement factor is 140 for η=3. Taking the orientation effect into account, an enhancement of about 400 is expected. These estimates are in good quantitative agreement with experiments.[19]

The calculations also quantitatively simulate the short-ranged enhancement shown in Fig. 3[20] and the linear relation between the enhancement and the background absorption by the island films. Note that the absorption calculated here is essentially that of metal island films and the vibrational spectrum is ascribed to the change in the absorption of the metal films at frequencies of adsorbate vibrations, from which the linear relation between the enhancement and the background absorption arises. The model calculations also well simulate ATR and external reflection SEIRA spectra.[29,39]

It is quite important to note that the model mentioned above predicts enhancement on transition metals as strong as on coinage metals.[21] For the electric field enhancement via localized plasmon, the real part of the dielectric function of the metal, $|\mathrm{Re}(\varepsilon_m)|$, must be much larger than the imaginary part, $\mathrm{Im}(\varepsilon_m)$.[1,2] Transition metals do not satisfy this requirement in the visible region and, hence, do not exhibit strong SERS. In the IR region, on the other hand, most metals satisfy the requirement. In fact, SEIRA has been observed not only on Ag and Au, but also on Pt,[12,14] Pd,[12] Ni,[12] Al,[14] In,[56] Cu,[56,57] and Pb.[58] Al, In, and Cu exhibit relatively small enhancement because the surfaces of the metals are easily oxidized in the air (note that the enhancement is short-ranged and, therefore, the enhanced electric field diminishes within the oxide layer).

The ATR measurements of thin organic films by using the prism/metal/air geometry (Kretschmann configuration) or prism/air/metal geometry (Otto configuration) have been extensively studied independently of SEIRA.[59] The metal films used in these experiments were continuous ones with thicknesses of a few hundred nm. When p-polarized light is incident at θ_c, photon and surface plasmon (of bulk metal) can couple to produce surface electromagnetic wave (SEW). SEW is nonradiative and propagates a few cm on the surface in the IR region. Vibrational spectra of molecules adsorbed on the surface can be obtained by measuring the attenuation of SEW. The absorption enhancement caused by the enhanced electric field of SEW has been investigated theoretically.[60,61] The sharp maximum at θ_c for p-polarization in Fig. 5b is ascribed to the excitation of SEW. However, the IR enhancement by SEW is not expected on island films because island dimensions are very much smaller than the propagation length of SEW. In fact, the SEW theory does not explain the experimental results described above.[9]

2.2. Chemical Models. There is a tendency for chemisorbed molecules to exhibit larger enhancement than physisorbed molecules, suggesting certain chemical contributions to SEIRA. One of the chemical origins is the orientation effect.[19] Chemisorption aligns the surface molecules. Preferentially oriented molecules give larger intensities than randomly oriented molecules for vibrations that give dipole changes normal to the surface due to the surface selection rule. The orientation effect functions destructively for molecular vibrations that give dipole changes parallel to the surface.

The increase in absorption coefficient (namely, dipole moment) of molecules upon chemisorption will also contribute to the enhancement. The absorption coefficient of CO, for example, increases by a factor of four by chemisorption on Ag.[62] Badilescu et al.,[63] and Merklin and Griffiths[64] suggested that vibrations of strongly polarizable groups within a molecule give larger enhancements than other groups, which was explained by donor-acceptor interactions with the metal surface.[64] In general, the contribution of the chemical effects seems to be much smaller than that of the electromagnetic effect. However, there exists a possibility that certain vibrational modes are significantly enhanced by chemisorption. Devlin and Constani[65] suggested that IR absorption can be enhanced through a vibronic coupling of vibrational modes with the charge-transfer between the adsorbed molecule and metal surface. The charge transfer enhancement has been observed for tetracyanoethylene anion radical[66] and thiocyanate[16] adsorbed on metal electrode surfaces. Totally symmetric modes that are originally IR-inactive for free molecules have been observed in the surface spectra, which has be ascribed to the vibronic coupling.[65] Despite the several intense studies, however, the chemical effect has not been fully elucidated and further study is desired.

3. Application to Electrochemistry

3.1. ATR-SEIRAS. In situ IR spectroscopy has provided extraordinary insights into the electrochemical interface, including the mechanisms of electrochemical reactions, adsorption/desorption behavior of molecules and ions, and double-layer structures.[67—69] The vast majority of in situ electrochemical IR studies have been carried out by means of IRAS. In the IRAS experiments, radiation from an IR source is reflected at the interface by being passed through the solution phase (Fig. 9a). Crucial to the success of this technique is the formation of a very thin (a few μm) layer of electrolyte solution between the IR window and the electrode by pressing the electrode against the window. This approach reduces the background absorption due to the bulk solution, which is very large in the case of aqueous solutions. However, several serious disadvantages arise from this geometry. Mass transport in and out of the thin layer is strongly restricted, resulting in the change of the interface including the local pH and concentrations. In addition, the time constant of the cell is very long due to the high resistivity. Reactions do not quickly respond to the externally applied potential changes. Furthermore, reactions occur first at the edge of the electrode and then gradually reach to the center of the electrode. Therefore, time-resolved IR monitoring often becomes meaningless except for very slow reactions.

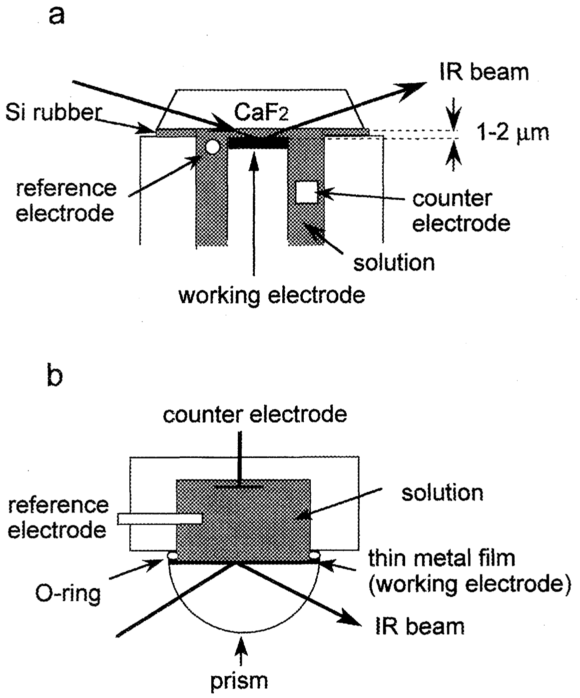

Fig. 9. Electrochemical cells and optical arrangements used for in situ characterization of electrode/electrolyte interfaces with IRAS and ATR-SEIRAS techniques (a and b, respectively).

The solution layer confined between the cell window and the electrode is very thin but is still much thicker than monolayer adsorbates, yielding the solution background several orders of magnitude larger than the signals from the interface. The so-called subtractively normalized interfacial FT-IR spectroscopy (SNIFTIRS) technique[67—69] is often used to remove the solution background by minimizing the spectral drift, which involves coadding sets of interferograms acquired at a suitable pair of electrode potentials and alternating the potential periodically. Nevertheless, since concentrations of ionic species in the diffusion layer change associated with potential changes, it is difficult to subtract the background completely. The question always arises in this type of work as to whether the observed bands are ascribed to adsorbed species or solution species, unless the peak frequencies of adsorbates bands and solution bands are well-separated. In addition, the SNIFTIRS technique can be used only for reversible systems.

One of the strategies to remove these problems is the use of the so-called Kretschmann ATR configuration (Fig. 9b). IR radiation is totally reflected at the interface by being passed through the ATR prism and, therefore, the solution phase is not necessary to be thin. Conventional ATR technique (without a metal film) has already been used at the beginning of IR studies of electrochemical reactions in the 1960's and 1970's.[70—72] However, this technique has a disadvantage that electrodes are limited only to conducting IR-transparent materials such as Ge and doped Si, because the ATR element serves as the working electrode. This problem can be solved by evaporating a thin film electrode onto the ATR element. The use of thin metal film provides an advantage to the ATR technique. Since the evanescent wave that penetrates into the solution phase is damped by the metal film,[57] the solution background is reduced significantly.[29]

The application of the Kretschmann ATR-IR technique to electrochemistry had been proposed in 1974 by Clarke et al.,[73] but was realized by the development of FT-IR instrumentation. In some of the in situ Kretschmann ATR-IR studies reported so far, relatively thick (a few hundreds nm) metal films were used as the working electrodes.[74—80] If an island film is used as the electrode, IR absorption of molecules in the very near vicinity of the electrode surface can be greatly enhanced due to SEIRA.[10,11,29] The signals from the interface and the solution background are comparable in the Kretschmann ATR-IR using thin metal films,[29] and thus the solution background can be canceled out very easily by taking a potential difference.[29,81] SNIFTIRS technique is not necessary in taking a potential difference, which is favorable for studies of irreversible reactions.[32,82] The most important advantage of the ATR-SEIRAS is that the strong surface signal enables time-resolved spectral measurements.[31,32]

The spectra of anthraquinone-2-carboxylic acid (AQ-COOH) adsorbed on Ag electrodes in 0.1 M (= mol dm^{-3}) $NaClO_4$ aqueous solution acquired with IRAS and ATR-SEIRAS techniques are compared in Fig. 10 (spectra a and b, respectively). The Ag electrode used in the IRAS measurement was a bulk plate, whereas that used in the ATR-SEIRAS measurement was a 20-nm thick film evaporated on a Ge prism. Very slow deposition of the metal is crucial to the success of this experiment (see Fig. 2). The conductivity of the evaporated metal film was good enough and no problems were found in electrochemistry. The spectra are shown in absorbance units defined as $-\log(R/R_0)$, where R and R_0 are the reflectivity at sample and reference potentials, respectively. The sample and reference potentials used in the measurements were −0.6 and −0.2 V, respectively, versus a Ag/AgCl(saturated) reference electrode. The spectra acquired with the two different techniques are essentially identical and it is apparent that ATR-SEIRAS has a sensitivity about 50 times higher than IRAS. The difference in the actual surface areas of the electrodes is only a factor of 2—3. The spectral region below 1100 cm^{-1} could not be observed by IRAS because of the cut-off of the cell window (CaF_2).

A clear difference is seen between the two spectra. The νCl–O mode of the supporting anion (ClO_4^-) is seen as a strong negative-going band at 1110 cm^{-1} in the IRA spectrum. The anion concentration at the interface increases as the applied potential is made more positive, yielding the negative-going anion band. On the other hand, the anion band is completely missing in the SEIRA spectrum, indicating that the very near vicinity of the surface is selectively monitored without the interference from the bulk solution.

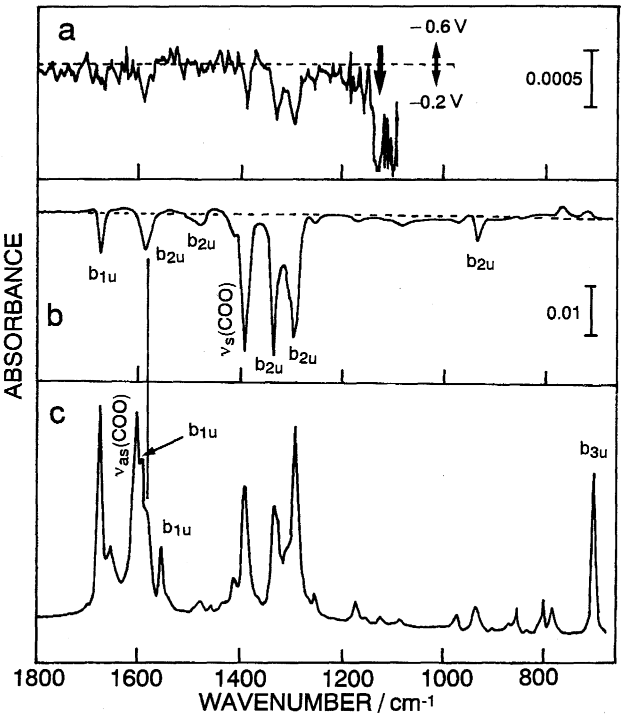

Fig. 10. Potential difference IRA (a) and ATR-SEIRA (b) spectra of anthraquinone-2-carboxylic acid adsorbed on bulk and evaporated Ag electrode surfaces, respectively, in 0.1 M $NaClO_4$. The spectra are shown in the absorbance units defined as $-\log(R/R_0)$, where R and R_0 are the reflectivity at −0.6 and −0.2 V (vs. Ag/AgCl), respectively. Trace c shows the transmission spectrum of the sodium salt of the molecule (KBr pellet).

AQ-COOH shows a quinone-hydroquinone type two-electron redox at −0.58 V, which is located between the sample and reference potentials. Therefore, the positive- and negative-going bands observed in the spectra are attributed to hydroquinone- and quinone-species, respectively. The strong negative-going band at 1392 cm^{-1} is assigned to the $\nu_s COO^-$ mode, indicating that the molecule is adsorbed on the electrode surface via the carboxyl group by releasing its proton. All the other negative-going bands are assigned to the fundamental modes of the aromatic ring.[29] The symmetries of the vibrations are shown in the figure under an assumption of D_{2h} symmetry by neglecting the carboxylato group. Compared with the transmission spectrum of the sodium salt of AQ-COOH (KBr pellet) shown in the figure (spectrum c), it is seen that the $\nu_s COO^-$ mode and b_{2u} modes of the ring are selectively enhanced. The asymmetric COO^- stretching ($\nu_{as}COO^-$) and b_{3u} modes (the CH out-of-plane bending modes) of the ring are completely missing in the surface spectra. On the basis of the surface selection rule, the result is interpreted that the molecule is oriented with the aromatic ring perpendicular to the surface, as illustrated in Fig. 11a. The vibrations classified into b_{1u}, b_{2u}, and b_{3u} give dipole changes along z, y, and x axes, respectively, where z and y axes are in the molecular plane and the z axis is taken along the two C=O bonds attached to the ring. The x, y, and z axes is inclined by 90°, 30°, and 60°, respectively, from the surface normal for this orientation. Therefore, the b_{2u} modes give the largest enhancement, while the b_{1u} modes give less enhancement and the b_{3u} modes no enhancement.

The reduced species, 9,10-dihydroxyanthracene-2-carboxylate, give only two weak positive-going bands at 780 and 757 cm^{-1} assignable to the CH out-of-plane bending modes, suggesting that the species is lying flat on the surface (Fig. 11b).

3.2. Real-Time Monitoring of Irreversible Reactions. The most frequently used electrochemical technique to study reactions is voltammetry, in which the electrode potential is swept linearly with time and current flow associated with reactions is measured. In order to collect spectra at every 10 mV during a potential sweep at 100 mV s^{-1}, for example, one spectrum must be collected within 100 ms. The time-resolution of a conventional FT-IR spectrometer is determined by the scan rate of the interferometer and millisecond time-resolutions have been achieved by the development of rapid scan FT-IR spectrometers. The maximum scan rate is 37 scans/s at a spectral resolution of 8 cm^{-1} for our FT-IR spectrometer (Bio-Rad FTS-60A/869), yielding the time-resolution of 27 ms.

Simultaneous IR and electrochemical measurements are useful in interpreting complicated reaction systems.[32] One example is shown for the irreversible redox reactions of 1,1′-diheptyl-4,4′-bipyridinium (better known as heptyl viologen; HV^{2+}) at a Ag electrode surface. It is known that HV^{2+} can exist in three redox forms, as a result of the following equilibrium:

$$\mathrm{HV}^{2+} + \mathrm{e}^- = \mathrm{HV}^{\cdot+}$$

$$\mathrm{HV}^{\cdot+} + \mathrm{e}^- = \mathrm{HV}^0.$$

In nonaqueous solutions, this molecule shows two well-separated pairs of redox waves in the cyclic voltammogram corresponding to the two one-electron redox reactions. In aqueous solutions, on the other hand, the voltammetric behavior is complicated, as shown in Fig. 12. The cyclic voltammograms were recorded in 0.3 M KBr solution containing 1 mM HV^{2+} with an evaporated Ag electrode at a potential sweep rate (v) of 10 mV s^{-1}. The potential was measured against a Ag/AgCl reference electrode. The radical cation, $\mathrm{HV}^{\cdot+}$, formed by the first reduction precipitates on the electrode surface at −0.52 V (wave a) as a blue-purple film due to the association with the supporting anion ($\mathrm{HV}^{\cdot+}\mathrm{Br}^-$). The neutral molecule, HV^0, is also insoluble in water and the blue-purple color of the $\mathrm{HV}^{\cdot+}$ film turns to yellow at −0.8 V. Note that the second reduction wave splits into two peaks (b and c). On the return positive scan, several oxidation waves d, e, f, and g are observed. Relative intensities of the peaks change with the sweep rate.[32] Since the reaction become less reversible as the sweep rate decreases, the complicated voltammetric behavior was ascribed to the "aging" (recrystallization or phase transition) of the deposited film. However, details of the aging effect has not yet been understood.

Figure 13 shows a series of IR spectra of the reduction products of HV^{2+} collected simultaneously with the cyclic voltammogram in Fig. 12. A spectrum acquired at −0.2 V, where the electrode surface is bare, was used as the reference. Each spectra were obtained without interferogram coaddition. The acquisition time of one spectrum was about 0.6 s, which is short enough to monitor the redox reactions. The dynamic spectra are different from the spectra acquired by means of IRAS technique by holding the potential at constant values,[83,84] because the products are aged during the spectral measurement in the latter experiments.

For direct comparison of the spectral and electrochemical data, the time-resolved spectra in Fig. 13 is shown in Fig. 14

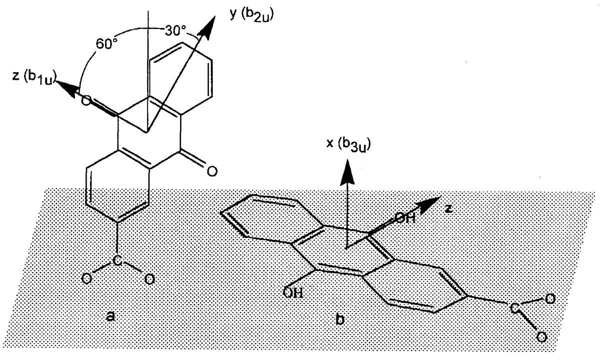

Fig. 11. Orientation of anthraquinone-2-carboxylic acid adsorbed on Ag electrode surface at potentials (a) positive and (b) negative of the equilibrium potential. The arrows indicate the directions of dipole changes associated with the ring vibrations classified into b_{1u}, b_{2u}, and b_{3u} symmetries under an assumption of D_{2h} symmetry by neglecting the carboxylato group.

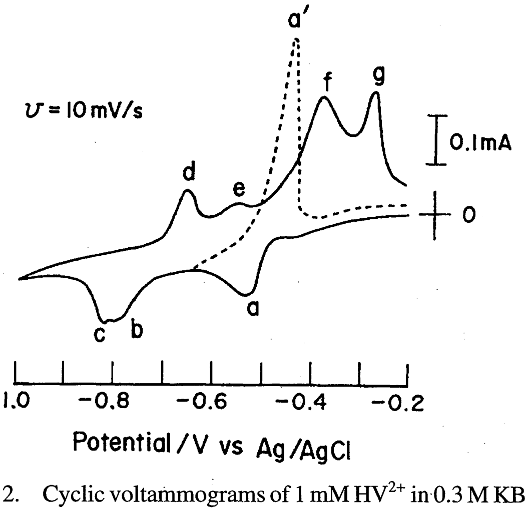

Fig. 12. Cyclic voltammograms of 1 mM HV^{2+} in 0.3 M KBr aqueous solution recorded with a Ag electrode at a sweep rates (v) of 10 mV s^{-1}.

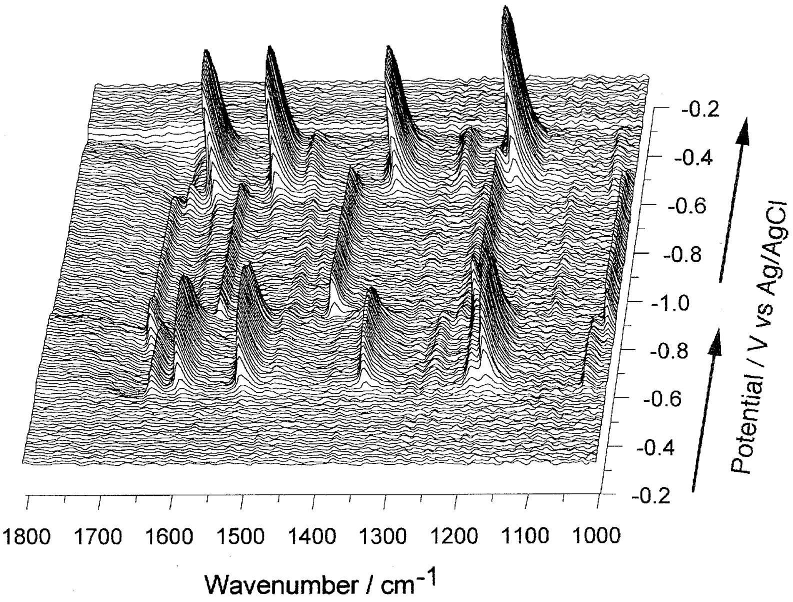

Fig. 13. A series of IR spectra for the HV^{2+} reduction at a Ag electrode collected simultaneously with the cyclic voltammogram in Fig. 12 (solid curve). Each spectrum was collected with a 0.6 s acquisition time.

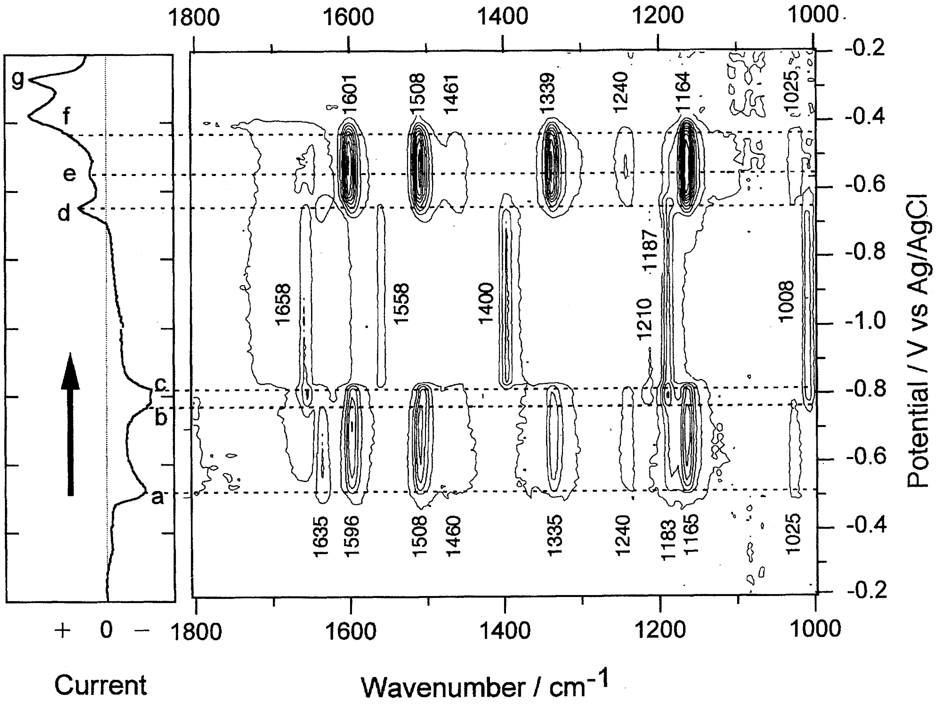

Fig. 14. A contour map of the time-resolved spectra in Fig. 13. The cyclic voltammogram is shown along the left side.

in a contour map and the cyclic voltammogram is shown at the left side of the map. It is apparent that large spectral changes occur around the potentials where redox waves appear in the voltammogram. The negative-going broad band around 1650 cm^{-1} is assigned to the bending mode of water (δHOH) removed from the interface by the deposition of the organic film.

On the potential sweep from −0.2 V to the negative direction, a set of bands attributable to $HV^{\bullet +}$ appear at about −0.5 V. Among these bands, the 1635 and 1183 cm^{-1} bands disappear at peak b. On the other hands, the other bands disappear at peak c. The different potential dependence of the observed bands suggests that two different species are formed by the first reduction and that the different reduction potentials of these species give two reduction peaks b and c around −0.8 V. In fact, the 1635 and 1183 cm^{-1} bands have been attributed to the monomer of the radical,[84)] whereas the other bands were attributed to the dimer of the radical with a plane-to-plane configuration linked by π-bonding.[83)] The dimer bands are assigned to the totally symmetric ring

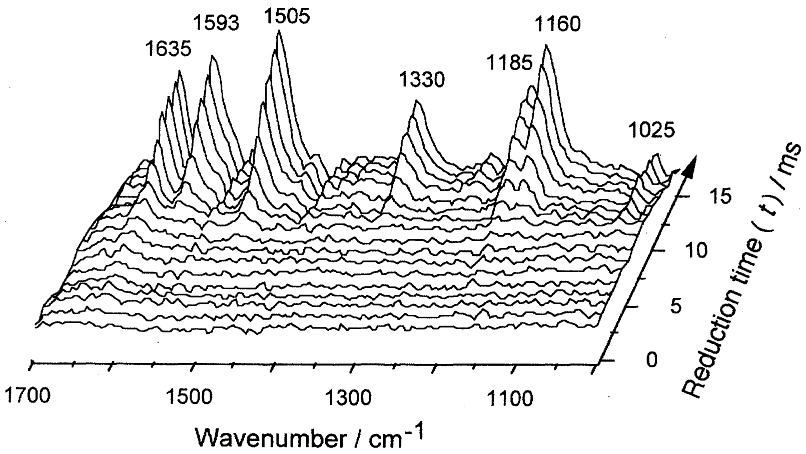

Fig. 15. Time-resolved IR spectra for the reduction of HV^{2+} to HV$^{\bullet+}$ at a Ag electrode for a potential step from −0.2 to −0.55 V (vs. Ag/AgCl). Each spectrum was collected with 100 μs acquisition time, but only the spectra of every 1 ms interval are shown for clarity.

vibrations.[32,83] The totally symmetric modes are originally IR-inactive in the D_{2h} symmetry of the molecule, but are activated and enhanced in intensity via vibronic coupling associated with charge transfer between the two paired radical molecules. On the other hand, the asymmetric modes are deactivated via vibronic coupling.[65] Therefore, the monomeric and dimeric radicals give greatly different spectra.

By the reduction of the HV$^{\bullet+}$ film at about −0.8 V, several bands attributable to HV^0 appear. The HV^0 generated from the monomeric HV$^{\bullet+}$ at wave b exhibits bands at 1658, 1210, 1187, and 1008 cm^{-1}, whereas the HV^0 generated from the dimeric HV$^{\bullet+}$ at wave c exhibits two bands at 1558 and 1400 cm^{-1}. This finding implies that two phases coexist also in the HV^0 film.

Corresponding to the two different phases of HV^0, two oxidation waves d and e appear in the voltammogram on the return positive-going sweep. The characteristic bands of the monomeric and dimeric radicals appear again at wave d and e, respectively, with consumption of HV^0 bands. It is interesting to note that the 1635 and 1183 cm^{-1} bands characteristic of the radical monomer completely disappear at wave e associated with the growth of the radical dimer bands. Since the monomeric radical is electrochemically stable at this potential range in the negative-going sweep (Fig. 12), the disappearance of the monomer bands is not due to the chemical reaction and is ascribed to the transformation of the monomer to the dimer. The phase transition is caused by the mismatch of the crystal structures of the two phases and/or by the π-interaction between the radicals being stronger than the coulomb interaction between the radical and anion.[32]

The dimeric radical bands completely disappear around −0.4 V due to the oxidation to HV^{2+} (at the negative-side shoulder of wave f). Nevertheless, large oxidation waves f and g are observed at more positive potentials in the cyclic voltammogram. The most plausible explanation of this puzzle is that the oxidation (dissolution) of the radical film initiates at the electrode/organic film interface and propagates outward towards the solution, since ATR-SEIRAS selectively probes the very near vicinity of the electrode surface (Fig. 3). This explanation is supported by the complete disappearance of the broad negative-going water band around 1650 cm^{-1}, indicating that water molecules are injected to the very near vicinity of the electrode surface.

When the negative potential sweep is limited to the first reduction (dashed curves in Fig. 12), the aging effect is negligible within a time-scale of a few tens seconds and the reaction is reversible. The dissolution of the unaged radical film initiates at the solution/organic film interface and propagates inward towards the electrode surface.[32] The different dissolution behavior of the radical films suggests that the unaged film has sufficient conductivity, whereas the aged film has poor conductivity. From a comparison of the IR and resonance Raman spectra of the radical, the change in conductivity was ascribed to the transformation of the monomeric radical to the dimeric radical (more exactly, the change in stacking of the molecules in the film).[32]

3.3. Microsecond Time-Resolved Monitoring by Step-Scan FT-IR. If the reaction to be studied is reversible or repeatable, microsecond time-resolved monitoring is possible by the use of step-scan FT-IR interferometry. The procedures to acquire time-resolved spectra by step-scan interferometry have been extensively described by Nakano et al.[85] Briefly, the step-by-step optical retardation change is achieved by a combination of a constant motion of the *moving* mirror and a sawtooth-like motion of the *fixed* mirror for our FT-IR spectrometer. First, the mirrors are stepped at the first optical retardation point X_1. After the mirrors are stabilized, the desired reaction is initiated via a potential step and the signal from the detector is collected at times t_1, t_2, $\cdots$, t_n with a constant time interval. Then, the interferometer is stepped forward to the second retardation point X_2, and the signal is accumulated following the same sampling sequence described above. This process is repeated until the optical retardation reaches its maximum value required for a specific spectral resolution. Thus obtained two-dimensional arrays of the time-dependent variation of the signal intensity $I(t_i)$ $(i=1-n)$ at each optical retardation X_j $(j=1-m)$ are rearranged to give interferograms $I(X_j)$ at each time t.

Finally, time-resolved spectra are given by FT of the time-resolved interferograms. The minimum time-resolution of our instrument, which is limited by the A/D converter used, is 5 μs.

The step-scan FT-IR spectrometry is useful to study very fast reactions. The first microsecond time-resolved IR monitoring was carried out to study the very initial stage of the HV^{2+} reduction to $HV^{\bullet +}$.[31] To minimize the aging effect, a short potential pulse from −0.2 to −0.55 V and back to −0.2 V with 20 ms width was applied. The result is shown in Fig. 15. The spectrum collected at −0.2 V was used as the reference. Each spectrum was obtained with 100 μs acquisition time, but only the spectra of every 1 ms interval are shown for clarity. The figure shows that a set of $HV^{\bullet +}$ bands grow in intensity with time t. The band intensities are well-correlated with the amount of the radical determined by chronocoulometry.[31] The intensity (and the charge consumed by the reduction) is proportional to $t^{3/2}$ at $t < 12$ ms and to $t^{1/2}$ at $t > 12$ ms, which indicates that the radical film is formed via an initial nucleation and subsequent diffusion-controlled film growth processes.

3.4. Two-Dimensional Correlation Analysis of Time-Resolved Spectra. Time-resolved IR spectroscopy provides dynamic and kinetic information on reactions. It will be useful to study short-lived reaction intermediates. However, the interpretation of the spectra is not easy if IR bands of reactants, intermediates and final products are highly overlapping. We have applied two-dimensional IR (2D-IR) technique to differentiate overlapping bands and to highlight dynamic and kinetic information involved in the time-resolved spectra.

The basic concept of 2D-IR is somewhat analogous to the 2D correlation technique used in NMR.[86—88] In 2D-IR, a spectrum defined by two independent wavenumbers is generated by a cross-correlation analysis of dynamic fluctuations of IR signals induced by a sample perturbation (e.g., potential modulation). Through the cross-correlation analysis, bands arising from different transient species are clearly differentiated by their characteristic time-dependent behavior.

The 2D correlation analysis shown below was carried out with the generalized 2D-IR formalism proposed by Nada.[88] Given a spectral intensity variation at a wavenumber ν for a period of time (t) between $-T/2$ and $T/2$, $y(\nu,t)$, the dynamic spectrum, $\tilde{y}(\nu,t)$, is defined as

$$\tilde{y}(\nu,t) = \begin{cases} y(\nu,t) - \bar{y}(\nu) & \text{for} - T/2 \leq T/2 \\ 0 & \text{otherwise} \end{cases}, \tag{7}$$

where $\bar{y}(\nu)$ is the time-average spectrum written as

$$\bar{y}(\nu) = \frac{1}{T}\int_{-T/2}^{T/2} y(\nu,t)\mathrm{d}t. \tag{8}$$

The correlation intensity between two arbitrary wavenumbers, ν_1 and ν_2, is defined as

$$\Phi(\nu_1,\nu_2) + i\Psi(\nu_1,\nu_2) = \frac{1}{\pi T}\int_0^{\infty} \tilde{Y}_1(\omega)\cdot\tilde{Y}_2^*(\omega)\mathrm{d}\omega, \tag{9}$$

where

$$\tilde{Y}_1(\omega) = \int_{-\infty}^{\infty} \tilde{y}(\nu_1,t)\mathrm{e}^{-i\omega t}\mathrm{d}t, \tag{10}$$

$$\tilde{Y}_z^*(\omega) = \int_{-\infty}^{\infty} \tilde{y}(\nu_2,t)\mathrm{e}^{+i\omega t}\mathrm{d}t. \tag{11}$$

The real and imaginary components of the correlation function, $\Phi(\nu_1,\nu_2)$ and $\Psi(\nu_1,\nu_2)$, are referred to, respectively, as the synchronous and asynchronous correlation. Synchronous and asynchronous 2D correlation spectra are constructed by plotting $\Phi(\nu_1,\nu_2)$ and $\Psi(\nu_1,\nu_2)$, respectively, over a spectral plane defined by the two independent (orthogonal) wavenumber axes, ν_1 and ν_2.

The synchronous 2D-IR correlation spectrum characterized the coherence of dynamic fluctuations of IR signals measured at two different wavenumbers. The synchronous correlation intensity becomes significant (i.e., nonvanishing) only if the time-dependent variations of the two IR signals are similar to each other. The asynchronous 2D-IR correlation spectrum is complementary to the synchronous 2D spectrum and characterizes the independent fluctuations of IR signals. The asynchronous correlation intensity vanishes unless the dynamic IR signals vary at different rates.

Synchronous and asynchronous correlations have either positive or negative sign. The sign of the synchronous correlation indicates the relative direction of change in dynamic spectral response. It is positive if the spectral intensities are changing (either increasing or decreasing) in the same direction. If the changes are in opposite directions, on the other hand, the sign becomes negative.

The sign of the asynchronous correlation provides the temporal relationship between the intensity fluctuations at ν_1 and ν_2. The sign is positive if the intensity fluctuation at ν_1 occurs before that at ν_2. If, on the other hand, the intensity fluctuation at ν_1 occurs after that at ν_2, the sign becomes negative. The temporal relationship described above must be reversed if the corresponding synchronous correlation intensity is negative.

The dynamic processes involved in the very initial stage of the HV^{2+} reduction were investigated by 2D-IR.[89] Figure 16a shows the synchronous 2D correlation spectrum constructed from the time-resolved spectra shown in Fig. 15. Normal IR spectrum of $HV^{\bullet +}$ (time-average spectrum, Eq. 8) is shown along the top and left sides of the 2D map for reference. Several peaks are developed at the frequencies of the bands observed in the original one-dimensional time-resolved spectra. The peaks located at diagonal positions, *autopeaks*, indicate that all the six bands change their intensities with t (namely, as the amount of the radical increases). The intense peaks appearing at off-diagonal positions, *cross peaks*, suggest that all the bands change their intensities simultaneously. Since the sign of the cross peaks is positive, the intensities of all the bands are changing in the same direction (increasing).

The corresponding asynchronous 2D correlation spectrum is shown in Fig. 16b. The shaded areas in the spectrum represent negative intensity regions. Asynchronous 2D correlation analysis provides deeper insight into the reaction dynamics. The 1636 and 1184 cm^{-1} bands, both assigned to the monomeric radical, have no asynchronous correlation

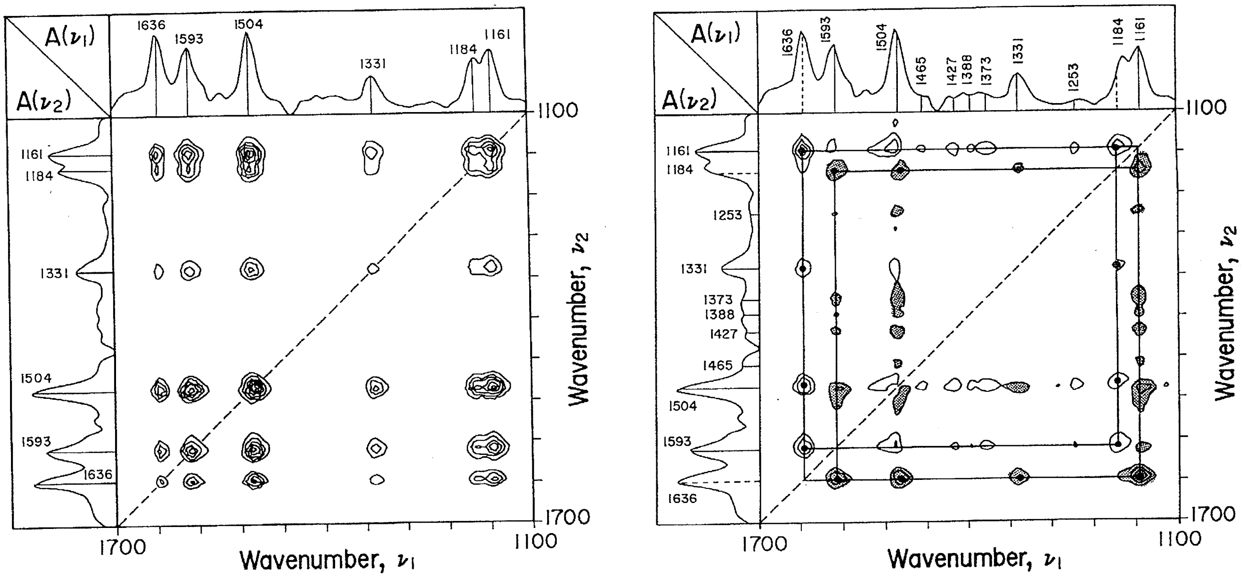

(a) (b)

Fig. 16. Synchronous (a) and asynchronous (b) 2D-IR correlation spectra of $HV^{\bullet +}$ constructed from the time-resolved spectra shown in Fig. 15. The shaded areas represent negative intensity regions.

with each other, indicating that the intensity changes of these two bands are completely synchronized. On the other hand, since these two bands have strong asynchronous correlation with the remaining four major bands at 1593, 1504, 1331, and 1161 cm^{-1} assigned to the dimer, the intensity changes of the monomer bands and the dimer bands are not completely synchronized. (Asynchronous 2D analysis judges the coherency and incoherency of the intensity changes more strictly than synchronous correlation analysis, which merely implies the existence of possible correlation between bands.[86,87]) Therefore, the cross peaks often appear at the same wavenumber coordinates in both synchronous and asynchronous spectra.) According to the above-mentioned rule regarding the sign of the cross peaks, it is concluded that the monomer bands appear earlier than the dimer bands.

Another notable observation in the asynchronous correlation 2D spectrum in Fig. 16b is the development of many weak cross peaks correlating the dimer bands. The cross peaks indicate that the dimer bands are composed of several components that change their intensities at different rates. To show this more clearly, the spectral region between 1610 and 1460 cm^{-1} is expanded in Fig. 17. The butterfly-like patterns along the diagonal line at about 1600 and 1500 cm^{-1} clearly show that these two bands are doublets; 1594 and 1581 cm^{-1}, and 1508 and 1497 cm^{-1} in peak positions. The presence of the lower frequency components is not clear in the one-dimensional spectra but is suggested from the asymmetric band shapes. The higher frequency components at 1594 and 1581 cm^{-1} have asynchronous cross correlations with the lower frequency components at 1581 and 1497 cm^{-1}. On the other hand, no cross peaks are found between the higher frequency components and between the lower frequency components. Therefore, these four bands are classified into two pairs by their characteristic time-dependent behavior. The sign of the asynchronous cross peaks indicates that the higher frequency components appear before the lower frequency components. Detailed analyses of the entire spectral region revealed that the other dimer bands at 1331 and 1161 cm^{-1} are also doublets. Since the vibrational properties of the $HV^{\bullet +}$ dimer are sensitive to the crystal structure (stacking of the molecules in the crystal),[32] the split of the dimer bands may be a scribed to the recrystallization in the deposited film.

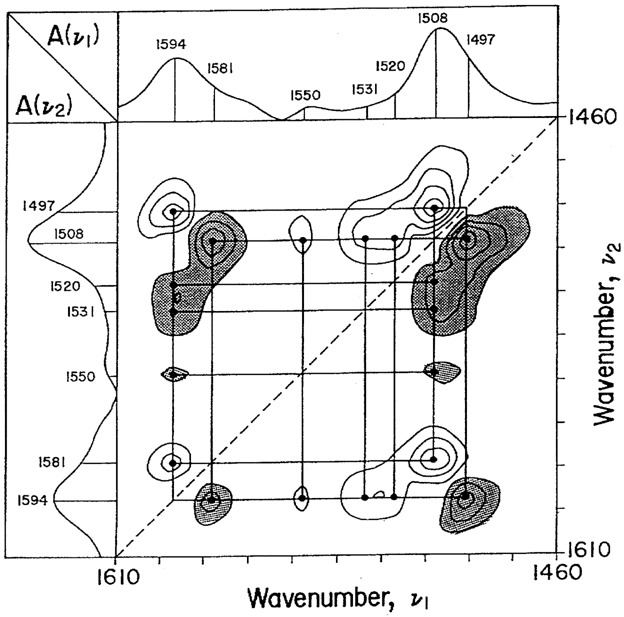

Fig. 17. Asynchronous 2D correlation spectrum of $HV^{\bullet +}$ constructed from the time-resolved spectra shown in Fig. 15. The shaded areas represent negative intensity regions.

Although 2D-IR correlation spectroscopy does not provide intrinsically new information that is not obtainable from usual one-dimensional spectra, it has an advantage of effectively accentuating certain useful information that are not distinctly seen in the one-dimensional spectra, as described above. The most important is that IR signals arising from different species can be clearly distinguished by their characteristic time-dependent behavior. Furthermore, the sequence of their intensity changes becomes clear. Such information is useful for detailed studies of reaction processes.

The 2D-IR correlation analysis has an additional advantage: it effectively enhances the signal-to-noise ratio of one-dimensional spectra. We detected very weak bands buried in very large noise signals by synchronous correlation analysis.[89,90] Since incoherent noise signals in each one-dimensional spectrum have no correlation with each other, they are canceled out by synchronous correlation analysis. The high noise-rejection ability of synchronous 2D spectrum is important for time-resolved IR studies because signal-to-noise ratios of spectra generally become worse as the time-resolution becomes higher. The signals that do not change in intensity with time are also rejected (see Eq. 7), which is useful to suppress the background absorption due to the bulk solution superposing on the surface signals.

Finally, it is important to point out that the *time* used in this 2D correlation analysis can be replaced by other reasonable variables.[88] It is possible to analyze a set of spectra collected, for example, at different potentials. In this case, the actual time sequence of data collection is no longer important, but the spectral data must be arranged in order of increasing or decreasing potential.

3.5. Double-Layer Structure at the Electrochemical Interface. Understanding the composition and structure of the electric double-layer formed at the electrochemical interface constitutes one of the major objectives in electrochemistry.[91] In particular, detailed knowledge of water molecules at the interface is an essential prerequisite to understanding electrocatalytic reactions. The adsorption of water molecules on metal surfaces has been studied extensively in ultrahigh vacuum (UHV) by means of modern surface analytical tools.[92] Since there exists a very strong electric field of about 10^7 $\mathrm{V\,cm^{-1}}$ at the electrode/electrolyte interface, however, the behavior or water at the interface will not be the same as that at the solid/vacuum interface. Classical models of the electrochemical interface assume that water molecules are ordered at the interface due to the strong electric field and reorient from "oxygen-up" to "oxygen-down" as the electrode charge (or, equivalently, potential) changes from negative to positive.[91] In the past decade, molecular dynamics simulations have come to be employed to investigate the structure and dynamics of water at electrified metal surfaces.[93,94] The computer simulations predict that water molecules are arranged in several layers from the surface and reorient depending upon the surface charge. The reorientation predicted is more complicated than that assumed in classical models. It has been predicted also that water molecules form an ice-like structure on uncharged and positively charged metal surfaces. The ordering of water molecules in several-layers has been confirmed on the Ag(111) electrode surface by means of in situ X-ray scattering.[95] However, the double-layer structure has not yet been fully elucidated.

ATR-SEIRAS probes the interface without the interference from the bulk solution and, hence, is very suitable to study the inner part of the double-layer (Helmholtz plane). We have investigated the potential-dependent reorientation of water molecules at the Au(111) surface in perchloric[81] and sulfuric acids[90] by this technique. Figure 18 shows a cyclic voltammogram of a 20 nm-thick Au film evaporated on a Si prism recorded in 0.5 M perchloric acid. The shape of the voltammogram is very similar to that recorded at the well-defined Au(111) single crystal surface. A STM observation of the evaporated thin film electrode revealed that the surface of each particle is constructed with the (111) terraces and steps. The broad peak around 0.8 V (vs. the reversible hydrogen electrode in the same solution, RHE) is due to the adsorption of perchlorate anion and the shoulder at the low potential side (at about 0.7 V) has been attributed to the lifting of the (1×23) reconstruction of the Au(111) surface to unreconstructed (1×1) phase.[96]

A series of IR spectra from the electrode surface in the perchloric acid, collected during a potential sweep from 0 to 1.3 V, is shown in Fig. 19. The spectrum acquired at the potential of zero charge (pzc) of the electrode (0.63 V) was used as the reference. The reference potential is chosen on the basis of molecular dynamics simulations,[93,94] which predict that water molecules are oriented flat on the electrode surface around the pzc. The flat-lying molecules do not give IR absorption because of the surface selection rule. Hence, the pzc is very suitable as the reference potential. The figure shows that the intensities and shapes of the νOH and δHOH modes of water change significantly as the potential changes,

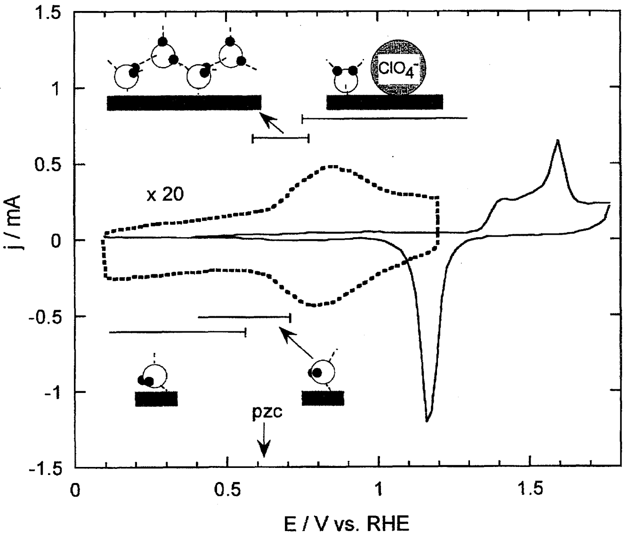

Fig. 18. Cyclic voltammogram of a vacuum-evaporated Au thin film electrode in 0.5 M $HClO_4$ at a sweep rate of 50 $\mathrm{mV\,s^{-1}}$. The insets show the orientation of water at the interface deduced from infrared spectra.

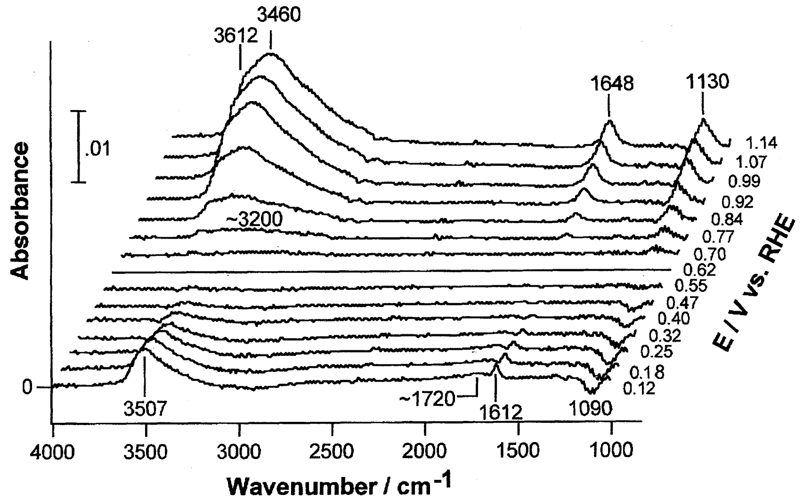

Fig. 19. A series of infrared spectra of a highly ordered Au(111) surface in 0.5 M $HClO_4$ as a function of applied potential. The reference potential is 0.62 V vs. RHE.

implying that the obtained spectra are of water molecules at the interface. To see the changes in more detail, the spectra at 0.12, 0.77, and 1.22 V are compared in Fig. 19 (spectra a, b, and c, respectively) by scaling the strongest bands to be equal. The spectra are apparently different from the transmission spectrum of bulk water (0.5 M perchloric acid, spectrum d) in both peak positions and shapes.

At potentials below 0.6 V where the electrode surface is charged negatively, the νOH and δHOH bands are shifted to higher and lower frequencies, respectively, compared with the bulk spectrum. In addition, the bands are apparently narrower. The shift and narrowing of the water bands are ascribed to the decrease in hydrogen bonding. It is noteworthy that the δHOH band is observed in the very low frequency region for water monomer and dimer (1595—1620 cm^{-1}), suggesting the interaction of water molecule with the metal surface via oxygen lone-pair orbital.[92] The findings are explained by assuming that each water molecule is oriented with both hydrogen atoms slightly closer to the surface than the oxygen atom (see Fig. 18). Note that hydrogen atoms are free from hydrogen bonding in this model due to the steric hindrance and only the oxygen lone-pair orbital directing toward the solution phase is available for hydrogen-bonding with a molecule in the second layer, which explains the relatively weak hydrogen-bonding.

The doubly degenerated asymmetric δHOH mode of oxonium (H_3O^+) is also observed in this potential range as a broad band at 1720 cm^{-1}. The corresponding symmetric δHOH mode was not observed in the expected range around 1150—1200 cm^{-1}. On the basis of the surface selection rule, the results indicate that oxonium is oriented with its C_3 axis nearly parallel to the electrode surface. Since oxonium with the assumed orientation is readily formed by adding the third proton to the oxygen lone-pair orbital directing toward the solution phase, the result seems to be very reasonable.

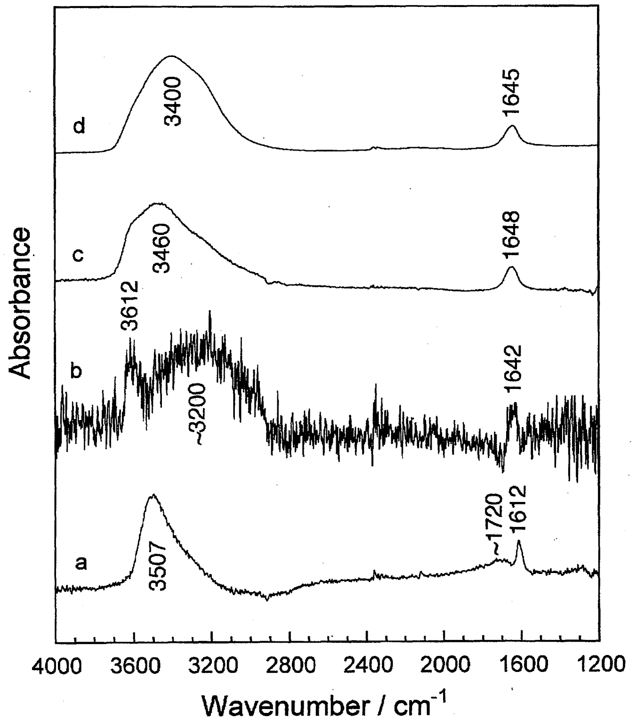

Fig. 20. Comparison of the water spectra at (a) 0.12, (b) 0.77, and (c) 1.22 V in Fig. 19. Spectrum d is the transmission spectrum of 0.5 M $HClO_4$. All the spectra are shown by scaling the strongest bands to be equal.

In the potential range slightly above the pzc, a broad and a sharp νOH band are observed at about 3200 and 3612 cm^{-1}, respectively (spectrum *b* in Fig. 20). Except for the latter sharp νOH band, the spectral feature is very similar to that of ice. The formation of ice-like structure at the electrochemical interface has been predicted by molecular dynamics simulations.[93,94] The ice-like structure is formed also on metal surfaces in UHV. The structure determined by means of modern surface analytical tools is essentially equivalent to the basal plane of ice I_h in contact with the surface.[92] The molecules in the first layer adjacent to the surface are oriented with hydrogen atoms slightly further away from the surface than the oxygen atom is, and a network of edge-sharing puckered hexagonal rings similar to that of the chair form of cyclohexane is formed by the hydrogen bonding with the second layer (see the inset in Fig. 18).

The very sharp band at 3612 cm^{-1} implies the presence of non-hydrogen-bonded OH moiety. This band grows in intensity with increasing the potential along with the growth of the 1090—1130 cm^{-1} band assigned to the νCl–O of adsorbed perchlorate anion. When the supporting anion is changed to chloride anion, this band shifts to 3592 cm^{-1}.[81] In sulfuric acid, this band was missing,[90] probably because of more significant red shift well into the broad νOH band region. Since perchlorate and chloride are hydrophobic and sulfate is hydrophilic, the anion dependence of the νOH band is ascribed to the difference in hydrogen-bond acceptability of the anions.

As the potential is made more positive than 0.8 V, an intense and broad νOH band appears at 3460 cm^{-1} and grows in intensity together with the sharp 3612 cm^{-1} band. The increase in intensity of the water bands suggests that the hydrogen-ends of water molecule orient more toward the solution phase. The change in the spectral feature around 0.8 V is well correlated with the adsorption of perchlorate anion,[81] suggesting that the anion adsorption changes the double-layer structure. The ratio of the integrated intensities of the sharp and broad νOH bands is 1 : 10. Since hydrogen bonding is known to increase the intensity of νOH band by a factor of 10, the numbers of free and hydrogen-bonded OH moieties are comparable. Similar spectral features have been observed for asymmetrically hydrogen-bonded water molecules (that is, only one OH moiety of a molecule is hydrogen-bonded) in organic solvents. Recalling that perchlorate is hydrophobic, it is believed that the one OH moiety adjacent to the adsorbed perchlorate is free from any hydrogen bonding and the other OH moiety is hydrogen-bonded with other molecules.

The potential-dependent reorientation of water molecules at the interface deduced from the IR spectra (see Fig. 18) is in good agreement with the molecular dynamics simulations of the electrochemical interface[93,94] except for the very positive potential region where anions are adsorbed. The effect of adsorbed anions is not taken into account in the computer simulations.

Very recently, we have succeeded in studying the dynamics of the water reorientation caused by a potential step at a time-resolution of 10 μs. When electrode potential is stepped from one to another, a current that exponentially decays with time is observed. The measurements of the transient current flow (chronoamperometry) is often used to obtain kinetic information on reactions and thermodynamic data for molecular adsorption.[34] The current flow has been interpreted by modeling the interface by an electrical circuit of a resister representing the solution resistance and a capacitor representing the double-layer at the interface. Time-resolved ATR-SEIRAS experiments were carried out to establish more realistic physical models for the transient current flow. The spectra from the Au(111) electrode surface in 0.5 M sulfuric acid showed that the reorientation of water occurs within the initial 1 ms and is followed by the adsorption of sulfate anion. The νSO band of adsorbed anion shifted to higher frequencies as coverage increases. When coverage of anion reached to about a half of full coverage, water molecules further reorient due to the hydrogen bonding with the anions. The dynamic changes of the interfacial structure terminated within about 3 ms, which was well-correlated with the transient current flow. This study is in progress and the details will be reported in a separate article.[97]

4. Summary and Remarks

The recent developments in SEIRA spectroscopy were reviewed. Two mechanisms are believed to contribute to the IR absorption enhancement: electromagnetic and chemical mechanisms. The origin of SEIRA is primarily ascribed to the local electric fields enhanced via the excitation of localized plasmon of small metal particles. Preferential orientation and the change in absorption coefficient of molecules caused by the chemisorption onto metal surfaces provide additional enhancements. The electromagnetic mechanism has been well established, whereas the latter chemical mechanism has not yet been fully elucidated.

By the use of SEIRA effect, electrode/electrolyte solution interfaces can be probed in situ at a very high sensitivity without the interference from the bulk solution. The utility of this technique was demonstrated for several electrochemical systems. The monitoring of the potential-dependent reorientation of water at the interface is one of the greatest achievements made by SEIRAS. This subject is very important in electrochemistry, but the thick solution phase has prevented the direct observation of the water layer adjacent to the electrode surface.

Time-resolved monitoring of electrochemical reactions at time-resolutions ranging from microseconds to milliseconds is also an important achievement made by SEIRAS. It is shown that IR and electrochemical simultaneous measurements provide significant insights into electrochemical reactions. Two-dimensional correlation analysis of time-resolved spectra provides further insights into reaction dynamics.

The success of the time-resolved IR monitoring is greatly owing to the development of time-resolved FT-IR instrumentation. Nevertheless, it must be noted that the signals from the interface must be strong enough to carry out time-resolved measurements. The time-resolved measurements with the step-scan mode shown in Fig. 15 required about 10 min for collecting all the data. Since the signal was strong enough, no signal averaging were carried out in this measurement. If the signals are weak and coaddition of a hundred to thousand interferograms are required to enhance the signal-to-noise ratio as in the case of IRAS, it will take 16.7 to 166.7 h to collect the data. Such long measurements are not impossible, but are not favorable because the electrode surface will be contaminated during the measurements. Therefore, the use of SEIRA is indispensable for time-resolved measurements.

In the course of the development of electrochemistry, advances have been made by the introduction of new diagnostic probes for analytical characterization of the interface. The author hope that the IR techniques described in this article will open up a new field in electrochemistry and related fields.

It is a pleasure to express my gratitude to many colleagues and collaborators who have stimulated and contributed much of the research described here, in particular to Dr. K. Ataka, Mr. K. Yoshii, Dr. Y. Nishikawa, Dr. I. Noda, Mr. T. Nakano, Dr. M. Ikeda, and Prof. T. Yotsuyanagi. The author's research were supported by Grants-in-Aid for Scientific Research (Nos. 06554033, 07640765, 08454171, 09218204, 09237101, and 09241201) and Grant-in-Aid for COE Research from the Ministry of Education, Science, Sports and Culture.

References

1) K. Chang and T. E. Furtak, "Surface Enhanced Raman Scattering," Plenum Press, New York (1982).

2) H. Metiu, *Prog. Surface Sci.*, **17**, 153 (1984).

3) A. Wokaun, "Solid State Physics," ed by H. Ehrenreich and D. Turnbull, Vol. 38, p. 223 (1984).

4) M. Moskovits, *Rev. Mod. Phys.*, **57**, 783 (1985).

5) A. Otto, I. Mrozek, H. Grabhorn, and W. Akemann, *J. Phys.: Condens. Matter*, **4**, 1143 (1992).

6) A. Hartstein, J. R. Kirtley, and J. C. Tsang, *Phys. Rev. Lett.*, **45**, 201 (1980).

7) A. Hatta, T. Ohshima, and W. Suëtaka, *Appl. Phys. A*, **A21**, 71 (1982).

8) A. Hatta, Y. Suzuki, and W. Suëtaka, *Apl. Phys. A*, **A35**, 135 (1984).

9) M. Osawa, M. Kuramitsu, A. Hatta, W. Suëtaka, and H. Seki, *Surface Sci.*, **175**, L787 (1986).

10) A. Hatta, Y. Chiba, and W. Suëtaka, *Surface Sci.*, **158**, 616 (1985); *Appl. Surface Sci.*, **25**, 327 (1986).

11) A. Hatta, Y. Sasaki, and W. Suëtaka, *J. Electroanal. Chem.*, **215**, 93 (1986).

12) Y. Nakao and H. Yamada, *Surface Sci.*, **176**, 578 (1986); *J. Electron Spectrosc. Relat. Phenom.*, **45**, 189 (1987).

13) T. Kamata, A. Kato, J. Umemura, and T. Takenaka, *Langmuir*, **3**, 1150 (1987).

14) T. Kamata, J. Umemura, and T. Takenaka, *Bull. Chem. Res. Kyoto Univ.*, **65**, 179 (1987).

15) Y. Suzuki, M. Osawa, A. Hatta, and W. Suëtaka, *Appl. Surface Sci.*, **33/34**, 875 (1988).

16) T. Wadayama, T. Sakurai, S. Ichikawa, and W. Suëtaka, *Surface Sci.*, **198**, L359 (1988).

17) A. Hatta, N. Suzuki, Y. Suzuki, and W. Suëtaka, *Appl. Surface Sci.*, **37**, 299 (1989).

18) W. Suëtaka, "Surface Infrared and Raman Spectroscopy: Methods and Applications," Plenum Press, New York (1995).

19) M. Osawa and M. Ikeda, *J. Phys. Chem.*, **95**, 9914 (1991).

20) M. Osawa and K. Ataka, *Surface Sci. Lett.*, **262**, L122 (1992).

21) M. Osawa, K. Ataka, K. Yoshi, and Y. Nishikawa, *Appl. Spectrosc.*, **47**, 1497 (1993).

22) Y. Nishikawa, K. Fujiwara, and T. Shima, *Appl. Spectrosc.*, **44**, 691 (1990).

23) Y. Nishikawa, K. Fujiwara, and T. Shima, *Appl. Spectrosc.*, **45**, 747 (1991).

24) Y. Nishikawa, Y. Ito, N. Yamakami, K. Fujiwara, and T. Shima, *Appl. Spectrosc.*, **45**, 752 (1991).

25) Y. Nishikawa, Y. Ito, N. Yamakami, K. Fujiwara, and T. Shima, *Surf. Interface Anal.*, **18**, 481 (1992).

26) Y. Nishikawa, K. Fujiwara, M. Osawa, and K. Takamura, *Anal. Sci.*, **9**, 811 (1993).

27) Y. Nishikawa, K. Fujiwara, and K. Takamura, *Bunseki Kagaku*, **43**, 425 (1994).

28) F. M. Hoffmann, *Surface Sci. Rep.*, **3**, 107 (1983).

29) M. Osawa, K. Ataka, K. Yoshii, and T. Yotsuyanagi, *J. Electron Spectosc. Relat. Phenom.*, **64/65**, 371 (1993).

30) R. Palmer, J. L. Chao, R. M. Dittmar, V. G. Gregoriu, and S. E. Plunkett, *Appl. Spectosc.*, **47**, 1297 (1993), and the references therein.

31) M. Osawa, K. Yoshii, K. Ataka, and T. Yotsuyanagi, *Langmuir*, **10**, 640 (1994).

32) M. Osawa and K. Yoshii, *Appl. Spectrosc.*, **51**, 512 (1997).

33) H. D. Abruña, "Electrochemical Interfaces: Modern Technique for In-Situ Interfaec Characterization," VCH, New York (1991).

34) J. Lipkowski and P. N. Ross, "Adsorption of Molecules at Metal Electrodes," VCH, New York (1992).

35) J. Lipkowski and P. N. Ross, "Structure of Electrified Interfaces," VCH, New York (1993).

36) Y. Nishikawa, T. Nagasawa, K. Fujiwara, and M. Osawa, *Vib. Spectosc.*, **6**, 43 (1993).

37) K. Ito, K. Hayashi, Y. Hamanaka, M. Yamamoto, T. Araki, and K. Iriyama, *Langmuir*, **8**, 140 (1992).

38) E. Johnson and R. Aroca, *J. Phys. Chem.*, **99**, 9325 (1995).

39) Y. Nishikawa, K. Fujiwara, K. Ataka, and M. Osawa, *Anal. Chem.*, **65**, 556 (1993).

40) For example: W. N. Hansen, *J. Opt. Soc. Am.*, **58**, 380 (1968).

41) M. Osawa and W. Suëtaka, *Surface Sci.*, **186**, 583 (1987).

42) J. R. Lombardi, R. L. Birke, T. Lu, and J. Wu, *J. Chem. Phys.*, **84**, 4174 (1986).

43) M. Osawa, N. Matsuda, K. Yoshii, and I. Uchida, *J. Phys. Chem.*, **98**, 12702 (1994).

44) G. A. Niklasson and C. G. Granqvist, *J. Appl. Phys.*, **55**, 3382 (1984), and references therein.

45) S. Yoshida, T. Yamaguchi, and A. Kinbara, *J. Opt. Soc. Am.*, **62**, 1415 (1972).

46) U. Laor and G. C. Schatz, *J. Chem. Phys.*, **76**, 2888 (1982).

47) H. Chew and M. Kerker, *J. Opt. Soc. Am.*, **B2**, 1025 (1985).

48) B. D. Chase and B. A. Parkinson, *Appl. Spectrosc.*, **42**, 1186 (1988).

49) A. Crookell, M. Fleischmann, M. Hannient, and P. J. Hendra, *Chem. Phys. Lett.*, **149**, 123 (1988).

50) C. Kittel, "Introduction to Solid State Physics," 7th ed, Weily, New York (1996), Chap. 13.

51) H. A. Pearce and N. Sheppard, *Surface Sci.*, **59**, 205 (1976).

52) C. F. Eagen, *Appl. Optics*, **20**, 3035 (1981).

53) E. C. Stoner, *Philos. Mag.*, **36**, 803 (1945).

54) P. B. Johnson and R. W. Christy, *Phys. Rev. B*, **B6**, 4370 (1972).

55) P. Schatz, S. Maeda, J. L. Hollenberg, and A. A. Dows, *J. Chem. Phys.*, **34**, 175 (1961).

56) M. Osawa, K. Ataka, M. Ikeda, H. Uchihara, and R. Nanba, *Anal. Sci.*, **7**, 503 (1991).

57) K. P. Ishida and P. R. Griffiths, *Anal. Chem.*, **66**, 522 (1994).

58) T. Yoshidome, T. Inoue, and S. Kamata, *Chem. Lett.*, **1997**, 533.

59) R. J. Bell, R. W. Alexander, Jr., C. A. Ward, and I. L. Tyler, *Surface Sci.*, **48**, 253 (1975); "Vibrational Spectroscopies

for Adsorbed Species," ed by A. T. Bell and M. L. Hair, American Chemical Soc., Washington, D. C. (1980), Chap. 6.

60) H. Ueba and S. Ichimura, *Surface Sci.*, **118**, L273 (1982).

61) Y. Ishino and H. Ishida, *Anal. Chem.*, **58**, 2448 (1986).

62) P. Dumas, R. G. Tobin, and P. L. Richards, *Surface Sci.*, **171**, 555 (1986).

63) S. Badilescu, P. V. Ashrit, V.-V. Truong, and I. I. Badilescu, *Appl. Spectrosc.*, **43**, 549 (1989).

64) G. T. Merklin and P. Griffiths, *Langmuir*, in press.

65) P. J. Devlin and K. Consani, *J. Phys. Chem.*, **85**, 2597 (1981).

66) S. Pons, S. B. Khoo, A. Bewick, M. Datta, J. J. Smith, A. S. Hinman, and G. Zachmann, *J. Phys. Chem.*, **88**, 3575 (1984).

67) A. Bewick and S. Pons, in "Advances in Infrared Raman Spectroscopy," ed by R. J. H. Clark and R. E. Hester, Wiley Heyden, Chichester (1985), Vol. 12, Chap. 1.

68) B. Beden and C. Lamy, in "Spectroelectrochemistry: Theory and Practice," ed by R. J. Gale, Plenum, New York (1988), Chap. 5.

69) R. J. Nichols, in Ref. 34, Chap. 7.

70) D. R. Tallant and D. H. Evans, *Anal. Chem.*, **41**, 835 (1969).

71) A. H. Reed and E. Yeager, *Electrochim. Acta*, **15**, 1345 (1970).

72) A. Z. Trifonov and I. D. Schopov, *J. Electroanal. Chem.*, **35**, 415 (1972).

73) J. S. Clarke, A. T. Kuhn, and W. J. Oliville-Thomas, *J. Electroanal. Chem.*, **49**, 199 (1974).

74) H. Neff, P. Lange, D. K. Roe, and J. K. Sass, *J. Electroanal.Chem.*, **150**, 513 (1983).

75) G. Nazri, D. A. Corrigan, and S. P. Maheswari, *Langmuir*, **5**, 17 (1989).

76) D. B. Parry, J. M. Harris, and K. Ashley, *Lamgmuir*, **6**, 209 (1990).

77) B. W. Johnson, J. Bauhofer, K. Doblhofer, and B. Pettinger, *Electrochim. Acta*, **37**, 2321 (1992).

78) E. Zippel, R. Kellner, M. Krebs, and M. W. Breiter, *J. Electroanal. Chem.*, **330**, 521 (1992).

79) D. Aurbach and O. Chusid, *J. Electrochem. Soc.*, **140**, L1 (1993).

80) I. Bae, M. Sandifer, Y. W. Lee, A. A. Tryk, C. N. Sukenik, and D. A. Scherson, *Anal. Chem.*, **67**, 4508 (1995).

81) K. Ataka, T. Yotsuyanagi, and M. Osawa, *J. Phys. Chem.*, **100**, 10664 (1996).

82) N. Matsuda, K. Yoshii, K. Ataka, M. Osawa, T. Matsue, and I. Uchida, *Chem. Lett.*, **1992**, 1385.

83) H. Sasaki, M. Takahashi, and M. Ito, *J. Electron Spectrosc. Relat. Phenom.*, **45**, 161 (1987).

84) S. H. Brienne, R. P. Cooney, and G. A. Bowmaker, *J. Chem. Soc., Faraday Trans.*, **87**, 1355 (1991).

85) T. Nakano, T. Yokoyama, and H. Toriumi, *Appl. Spectrosc.*, **47**, 1374 (1993).

86) I. Noda, *Appl. Spectrosc.*, **44**, 550 (1990).

87) I. Noda, A. E. Dowrey, and C. Marcott, *Appl. Spectrosc.*, **47**, 1317 (1993).

88) I. Noda, *Appl. Spectrosc.*, **47**, 1329 (1993).

89) M. Osawa, K. Yoshii, Y. Hibino, T. Nakano, and I. Noda, *J. Electroanal. Chem.*, **426**, 11 (1997).

90) K. Ataka and M. Osawa, submitted to *Langmuir*.

91) J. O'M Bockris and S. U. M. Khan, "Surface Electrochemistry: A Molecular Level Approach," Plenum Press, New York (1993).

92) P. A. Thiel and T. E. Madey, *Surface Sci. Rep.*, **7**, 211 (1987), and references therein.

93) G. Nagy and K. Heinzinger, *J. Electroanal. Chem.*, **296**, 549 (1990); **327**, 25 (1992).

94) K. Heinzinger, in Ref. 35, Chap. 7.

95) M. Toney, J. N. Howard, J. Richer, G. L. Borges, J. G. Gordon, O. R. Melroy, D. G. Wiesler, D. Yee, and L. B. Sorensen, *Nature*, **368**, 444 (1994); *Surface Sci.*, **335**, 326 (1995).

96) D. M. Kolb and J. Schneider, *Electrochim. Acta*, **31**, 929 (1986), and in Ref. 35, Chap. 3.

97) K. Ataka and M. Osawa, to be published.

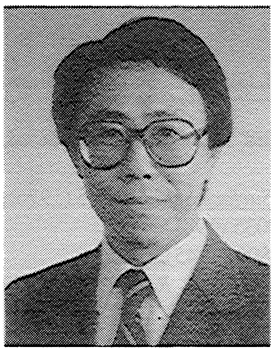

Masatoshi Osawa was born in Akita in 1950. He was graduated from Tohoku University in 1974 with bachelor degree in material engineering. He also received his master degree in material engineering in 1976 from the same university. After the graduation of the master course, he was appointed as a Research Assistant of Tohoku University. In 1984, he received Doctor of Engineering degree from Tohoku University under the direction of Professor Wataru Suëtaka. He was promoted to Associate Professor of Tohoku University in 1989. In 1994, he moved to Catalysis Research Center of Hokkaido University as Professor. He spent one year from 1984 at IBM San Jose Research Laboratories (now Almaden Research Center) as a Visiting Scientist. His current research interest is in the area of physical electrochemistry, especially spectroscopic characterization of the electrochemical interface.